Wave overtopping flow striking a human body on the crest of an impermeable sloped seawall. Part I: physical modeling

Deping Cao[a], Jing Yuan[1a], Hao Chen[b], Kuifeng Zhao[a], Philip Li-Fan Liu[a]

[a]*Department of Civil and Environmental Engineering, National University of Singapore, 1 Engineering Dr. 2, Block E1A 07-03, Singapore 117576*
[b]*School of Engineering, University of Glasgow, Glasgow, UK*

Abstract

The present paper is the first of two companion papers on the investigations of wave overtopping flow striking a cylinder, which is the schematisation of a human body, on the crest of an impermeable sloped seawall with a deep foreshore. This paper presents the physical modelling part. The key measured physical quantities include the overtopping flow depth on the seawall crest and the inline force on the cylinder. It is found that the Iribarren number and the ratio of freeboard and incident wave height are the two key parameters that control wave breaking on the seawall slope and the overtopping flow on the seawall crest. Formulas are identified for quick estimation of the inline force due to overtopping flow. The maximum overtopping flow depth and the maximum inline force are found to decay exponentially with the distance from the seawall's edge, but the decay rates are rather low. By comparing the inline force experienced by a 3D-printed human model and a cylinder, the equivalent diameter of a human body is proposed to be 1.4 times the thigh

[1]Corresponding author, Email: nusyuan@gmail.com

width. Finally, a preliminary application was carried out to demonstrate the applicability of our research outcomes. It is found that the predicted maximum inline force on a human body exceeds the ground friction, when the smallest overtopping volume exceeds about 600 l/m (with a scatter range of 600 to 1100 l/m), which is conservatively in consistent with the threshold proposed in the EurOtop manual.
Keywords: overtopping flow depth, inline force, 3D-printed model, overtopping volume limit, pedestrian safety

---

1. Introduction

Seawalls are common coastal structures for protecting properties and people near the waterfront from wave actions. Wave-induced overtopping flow occurs when the wave runup is higher than the seawall's freeboard, and it cannot be fully avoided as the sea level and incoming wave conditions are subjected to large variabilities. Wave overtopping may be a great threat to the pedestrians standing on the seawall crest. It has been reported that many people died due to wave overtopping or wave actions on seawalls and other similar coastal structures in UK between 1999 and 2002 (Allsop et al., 2003) and in 2005 (EurOtop, 2018). Therefore, it is important to ensure that the coastal seawalls are properly designed or managed to protect pedestrians from being injured by the overtopping flow. In the context of global climate change, we expect to experience harsher wave conditions and rising sea level, so it is also necessary to have good tools for assessing whether the existing seawalls are sufficiently safe for allowing public access in the future. Tolerable overtopping conditions depends on the type of seawall. In this study we

focused on sloped seawalls.

Understanding the overtopping process is the first step to assess and manage the overtopping risk. There are numerous studies in the literature on overtopping flow on the horizontal crest of a sloped seawall. Most of these studies focus on the overtopping discharge rate and overtopping volume (e.g. Goda, 2009; Nørgaard et al., 2014; Van Doorslaer et al., 2015; Pan et al., 2015; Hughes and Thornton, 2016; Molines et al., 2019; EurOtop, 2018; Salauddin and Pearson, 2019). Various equations have been proposed to estimate the overtopping flow discharge rate and overtopping volume for a sloped seawall, most of which have been well summarized in the manual by EurOtop (2018) (hereafter EurOtop 2018). A few studies (e.g. Van Gent, 2003; Schüttrumpf and Oumeraci, 2005; Van der Meer et al., 2011; Chen et al., 2015; Mares-Nasarre et al., 2019; Van Bergeijk et al., 2019) investigated overtopping flow depth and overtopping flow velocity on the horizontal crest of the seawall. Schüttrumpf and Oumeraci (2005) theoretically derived a set of formulas for the prediction of maximum overtopping flow depth at the leading edge on the crest and the landward slope of a dike and validated them experimentally. Chen et al. (2015) experimentally studied the overtopping flow features and impact force on a vertical wall installed on a dike with a very shallow foreshore. The decay of overtopping flow depth with the distance to the crest's edge was studied by many researchers (e.g. Van Gent, 2003; Schüttrumpf and Oumeraci, 2005; Van der Meer et al., 2011), and most studies adopt an exponential decay function with different choices of length scale.

EurOtop (2018) provided tolerable overtopping conditions in terms of

threshold values of the mean overtopping discharge rate and maximum overtopping volume for various incident wave heights, but these conditions were not developed based on detailed studies of flow-human interaction. There are some published studies that investigated how overtopping flows interact with structures on a seawall crest. De Rouck et al. (2012) performed large scale laboratory tests on the overtopping flow impact on a storm wall. Chen et al. (2015) experimentally studied the overtopping impact force on a vertical wall on the crest of a sloped seawall. Based on the concept of depth-integrated momentum flux, they derived a semi-analytical formula for the inline force on a vertical wall caused by the overtopping flow. In both studies (De Rouck et al., 2012; Chen et al., 2015), the flow-structure interaction can be considered as 2-dimensional, since a vertical wall fully blocks the overtopping flow. However, the flow-human interaction is akin to 3-dimensional flow-cylinder interaction. The flows can go around the human body and form a wake, which is absent for a vertical wall. Endoh and Takahashi (1994) firstly conducted some flume experiments on flow striking human bodies. They also studied the danger of a person being carried into sea by overtopping flow on a caisson breakwater. Unfortunately, very few such studies on overtopping-flow-human interaction are available in the literature.

There are indeed some studies on other type of flow (e.g., flood flow) interacting with human body. Arrighi et al. (2017) numerically studied the instability of a human body subjected to a flood flow and they developed an index parameter that accounts for both flow and human body characteristics to assess instability of the person. Some researchers (e.g. Foster and Cox, 1973; Abt et al., 1989; Jonkman and Penning-Rowsell, 2008; Martínez-

Gomariz et al., 2016) reported real-human experiments, most of which were conducted in flume or basin, where the water depth and flow velocities were well controlled. The steady flows in those studies are fundamentally different from the overtopping flow, which is highly transient (i.e., both flow depth and velocity change within a few seconds). Thus, the guidelines for people's safety in flood flows cannot be directly applied to overtopping flows.

To limit the scope, we consider a sloped seawall with a smooth surface in the present study, and we assume the water depth at the toe of the structure is large enough for neglecting an influencing foreshore. Some examples of such seawalls are the revetments commonly seen in Singapore, of which the gaps of the ripraps are carefully filled with mortar, leading to a smooth seawall surface (see Fig. 1 for an example). The human body is conceptualized as a circular cylinder. This simplification has been widely adopted, e.g., in Lind et al. (2004) and Jonkman and Penning-Rowsell (2008), and it can significantly ease the setup of both numerical and physical modeling. In this study, some additional comparative laboratory tests, which compares the inline force on a cylinder and a 3D-printed human model, were performed to validate the simplification. The location where pedestrians stand on the seawall crest can potentially affect the inline force, so the variation of inline force with the location of the cylinder is also studied in the present study. This paper is the first of two companion papers, which is mainly on physical modelling of the flow-cylinder interaction process on a 1-on-3 slope. The second paper (Chen et al., 2021) presents a high-fidelity numerical simulation to reveal the detailed hydrodynamic process for various slopes, which also enlarges the data set.

The main objective of the present paper is to develop an easy-to-use formula for the estimation of the inline force on the human body due to overtopping flow. The remaining of the paper is organized as follows. Section 2 presents a dimensional analysis that guides the whole study, while Section 3 describes the physical model. The experimental results on overtopping flow depth and the inline force are presented in Section 4. Also in this section, two alternative formulas for the maximum inline force are developed and the effects of cylinder location are also discussed. In Section 5, the experiments using a 3D-printed human model are presented and the equivalent diameter of a human body is discussed. A preliminary application of the research outcomes is presented in Section 6. Finally, the conclusions are given in Section 7.

2. Scaling laws

The target of the paper is to evaluate the risk of a pedestrian being striken away by an overtopping flow. Two failure modes, namely "sliding mode" and "overturning mode", have been reported in the literature (e.g. Foster and Cox, 1973; Abt et al., 1989; Jonkman and Penning-Rowsell, 2008; Martínez-Gomariz et al., 2016). Foster and Cox (1973) and Martínez-Gomariz et al. (2016) have reported that most failure cases of people being in high speed and shallow flow are due to "sliding mode", where the flow drag force is larger than the ground friction force. For overtopping flow considered in this study, it is assumed that flow speed is very high and flow with a small depth (20∼40 cm) can lead to a large enough striking force to move a pedestrian. This is similar to flooding flow reported by Martínez-Gomariz et al. (2016), although

overtopping flow is transient with a duration of $\mathcal{O}(1s)$. This assumption of high speed overtopping flow and shallow overtopping flow depth will be verified later by our experimental results in Section 4.

The key physical parameter for the risk assessment of overtopping flow is the maximum inline force (which is the overtopping striking force in the streamwise or overtopping flow direction), F_{0m}, acting on a cylinder located at the edge of the seawall (see Fig. 2 for the definitions of the variables). In this study, we define the edge as 1.5 times cylinder diameter from the actual leading edge, i.e., $x_c = 1.5D$, where $x_c = 0$ cm is the actual leading edge and D is the cylinder's diameter. The reasons for employing the definition of "edge" are as follows. At the actual leading edge, the water flow transits from the run-up flow on the slope to a horizontal overtopping flow on the crest and this transition is heavily affected by the detailed local geometry at the joint, which is not considered in this study. Also, the actual leading edge is always unsafe for people to stand there, with or without an overtopping flow.

To account for the fact that F_{0m} increases with the cylinder's diameter D, we further introduce a maximum inline force per unit diameter, i.e., $F^* = F_{0m}/D$, as the target variable. Apparently, F^* depends on a set of variables, which describe wave condition, seawall design, property of the fluid, and the size of the cylinder. Assuming normal incident long-crested waves, the wave condition is simply governed by the wave height H and wave period T. The sloped seawall is characterized by the slope β and the freeboard R_c. The roughness of the slope is neglected here for simplicity. The property of the fluid is described by the fluid density ρ and the fluid kinematic viscosity ν.

This size of the cylinder is characterized by its diameter D. Finally, the gravitational acceleration, g, is also a relevant variable.

The dependent variable F^* is related to 8 independent variables, i.e., $F_{0m} = f(H, T, R_c, \tan\beta, \rho, \nu, g, D)$. The independent variables and F_{0m} are converted into the following six dimensionless parameters:

$$\pi_1 = \frac{F_{0m}}{\rho g H^2}, \pi_2 = \frac{gT^2}{H}, \pi_3 = \frac{R_c}{H}, \pi_4 = \tan\beta, \pi_5 = \frac{\sqrt{gH^3}}{\nu} \text{ and } \pi_6 = \frac{D}{H} \quad (1)$$

Here π_5 is a Reynolds number, which describes the role of viscous effect in the system. The inline force is due to a thin layer of high-speed flow striking on the cylinder, which is an inertia-dominated process, so π_5 should have an insignificant role in the system. π_6 compares the diameter of the cylinder to the incident wave height. In the background problem of overtopping flow hitting a human body, a very small wave height gives little inline force, while a very large wave height surely produces an inline force far exceeding the tolerable value, so we can limit our study to wave height within 0.5 to 2 m (following the tolerable overtopping conditions in EurOtop 2018). As will be discussed in Section 5, the equivalent diameter of human body is about 20$\sim$40 cm. Thus, the variability of π_6 is limited, so we can also assume that π_6 does not affect the system's behavior. π_2 and π_4 can be combined and converted into the Iribarren number, I_r ($= \tan\beta/\sqrt{H/L_0}$, where L_0 is the deep water wave length). Thus, the normalized maximum inline force is determined as,

$$\frac{F^*}{\rho g H^2} = f_{F0m}(I_r, \frac{R_c}{H}, \tan\beta) \quad (2)$$

Eq. (2) implies that the maximum inline force only depends on the wave breaking (I_r number), the slope of the seawall and the relative freeboard.

Eq. (2) can be further written as,

$$F_{0m} = f_{F0m}(I_r, \frac{R_c}{H}, \tan\beta)\rho g H^2 D \tag{3}$$

Chen et al. (2015) experimentally studied the overtopping flow force on a vertical wall on two different slopes ($\cot\beta = 3$ and 6) and obtained an empirical relationship between F_{0m} and β. Following Chen et al. (2015), we assume that the F_{0m} is scaled with $1/\tan\beta$, so we can eliminate F_{0m}'s dependency on $\tan\beta$, and finally a scaling for F_{0m} is obtained as

$$F_{0m} = C_H(I_r, \frac{R_c}{H})\cot\beta\rho g H^2 D \tag{4}$$

where C_H is a scaling parameter. This formula takes the wave height H as the representative length scale of the flow, so we hereafter refer to it as the H-scaling. It is easy to use if individual wave (in terms of H and T) at the toe of the seawall is known, but it does not explicitly involve any parameter that describes the overtopping flow. In recent years, RANS-based numerical models are becoming popular tools for overtopping studies (e.g. Higuera et al., 2013, 2014). These models can directly resolve the overtopping flow, so it is interesting to provide an alternative that explicitly involves some physical parameters describing the overtopping flow. To this end, we choose the maximum overtopping flow depth at the seawall's leading edge, d_{0m}, as a bulk parameter of the overtopping flow. It can be seen that d_{0m} is a function of the 7 independent variables (H, T, $\tan\beta$, R_c, ρ, ν, g). A dimensional analysis for d_{0m} (similar to that for F_{0m}) yields

$$d_{0m} = f_{d0m}(I_r, \frac{R_c}{H}, \tan\beta)H \tag{5}$$

Combining Eqs. (2) and (5), and assuming that the effect of $\tan\beta$ can be described as the $\cot\beta$ term in Eq. (4), we can derive another formula for

F_{0m}, i.e.,

$$F_{0m} = C_d(I_r, \frac{R_c}{H}) \cot\beta \rho g {d_{0m}}^2 D \tag{6}$$

where C_d is a scaling parameter. Here d_{0m} is taken as the representative length scale, we shall hereafter refer to Eq. (6) as the d-scaling.

It should be noted that no overtopping flow velocity u is included in Eqs. (4) and (6). This is because the maximum inline force is scaled with momentum flux of overtopping flow, $M = u^2 d$. The overtopping flow depth is scaled with H which is controlled by R_c/H and I_r. The terms u^2 which represents the kinetic energy of overtopping flow, is scaled with $(R_u - R_c)$, where R_u is scaled with $I_r H$ (Schüttrumpf and Oumeraci, 2005). Thus it can be derived that M is scaled with d^2 or H^2. And the scaling parameters (C_d and C_H) are functions of R_c/H and I_r.

A key target of this paper is to derive the scaling parameters in Eqs. (4) and (6) based on our wave-flume experiments.

3. Experiments

3.1. Experiment setup

Experiments were conducted in a wave flume in the Hydraulics Laboratory at National University of Singapore. This wave flume is 36 m-long, 1.3 m-deep and 2 m-wide. A piston-type wave maker supplied by HR Wallingford for generating waves is located at one end of the flume. Near the other end of the flume, the sidewalls are made of glass, allowing sideview observations and measurements. Since the target waves to be simulated in this study is around 1 m, and a typical height of a seawall (from crest to toe) in Singapore is about 4 m, the size of this flume allows a geometric scale

around 1:5. The seawall model consists of a 1-on-3 frontal slope and a flat crest, which mimics typical revetments in Singapore. The sketches of the setup in front and top view, the photo of the seawall model, cylinder model and the force sensor and the whole wave flume are provided in Figs. (a), (b), (c), (d) and (e) in Fig. 3, respectively. The model was installed with its toe at 23.57 m downstream of the wave maker. Two large pieces of glass were joint together to form the model's front slope (1:3) and the crest. Note that in the present study, we used a slope made of glass to model actual revetment as shown in Fig. 1. The roughness of the actual slope is larger than glass, so some future studies are required to further investigate the roughness effect. The glass plates were supported by a metal frame from underneath. The joint was sealed with silicon to ensure a smooth transition. The glass plates spanned the whole width (2 m) of the flume, and the gaps with the sidewalls of the flume were sealed with silicon for water proofing. The seawall crest is 1 m long and 2 m wide. A water collection tank, which is 1.91 m wide, 0.96 m long and 0.7 m deep, was attached to the rear of the model. The gaps between the sidewalls of the collection tank and the flume walls were sealed, so the overtopping water can be collected in this tank. Thus, the overtopping flow rate can be easily estimated from the volume of water collected in the tank.

A cylinder, as a surrogate of human body, was placed on the model seawall crest. The cylinder model was made of plastic pipe with an outer diameter of 6 cm, which gives a geometric scale around 1:5 (assuming that the width of human's lower body is around 20$\sim$40 cm). The upper end of the pipe was mounted to a three-axis force sensor which was bolted onto a rigid bar

sitting on top of the flume. There was a tiny gap between the bottom of the cylinder and the seawall surface. This tiny gap ensures that the cylinder will not touch the seawall surface during an experiment. Moreover, the distance of the cylinder model from the leading edge of the seawall crest can be varied to investigate the effect of location.

3.2. Measurement instruments

The physical quantities measured in this study are: (a) free surface elevation in the flume, (b) depth of overtopping flow on the seawall crest, (c) the volume of overtopping flow, (d) inline force on the cylinder.

Four capacitance type wave gauges were installed to measure the surface elevations at a few selected locations. The gauges can measure a maximum wave height of 40 cm with an uncertainty of about 1 mm. A wave gauge (named as CG1) was installed at $X = 6.55$ m downstream from the wave paddle for monitoring the wave generation ($X = 0$ m is the mean location of wave maker, and X increases towards the seawall model). Two gauges (CG2 and CG3) were installed in the middle of the flume (X =17.29 and X =17.83 m) for determining the incident and reflected waves through wave reflection analysis (see Section 3.4 for more details). The fourth one, CG4, was installed at the toe position (X =23.57 m) for monitoring the wave condition right in front of the seawall model. Finally, a fifth wave gauge, CG5, was installed in the collection tank to measure the water accumulation in the tank.

Four ultrasonic probes (noted as US1 to US4) were used to measure the depth of overtopping flow on the seawall crest. These probes were hanged above the free surface. They send out pulses of acoustic signals, which travel downwards to the water surface and then get reflected back. Based on the

arrival time of reflected signal, the vertical level of the free surface is determined. The units were aligned along the flume's longitudinal direction, and were placed 0.7 m from the flume wall (or 0.3 m from the cylinder), as shown in Fig. 3. The space between two neighbouring probes was 18 cm along the X direction. Note that US1 was installed right at the leading edge of the seawall crest, so US4 is 54 cm from the leading edge.

A Sony high-speed camera, with a sampling rate of up to 100 frame per second and a resolution of 1920×1080 pixels, was used to capture the process of overtopping flow and running up on the cylinder.

A three-component load cell (LSM-B-SA1, KYOWA) was deployed for measuring the force acting on the cylinder. This unit is a strain gauge based 3-component force transducer for simultaneously measuring force in 3 directions. It has a measuring capacity of 50 N and a natural frequency of 800 Hz. The measurement was sampled at a frequency of 200 Hz.

A National Instrument (NI) data acquisition system was used to synchronize the signals of wave gauges, ultrasonic probes and force sensor. The captured videos were synchronized with other instruments by identifying the moment that overtopping flow first crosses the leading edge of the seawall crest.

3.3. Test conditions

Totally 203 tests with different wave conditions, freeboard and location of the cylinder were performed in this study. All experiments in this study were with regular waves. As listed in Table 1, the model wave height, H, was between 0.069∼0.209 m, and the model wave period, T, was between 1.2∼3 s, which is determined to make the model wave length follow the geometric

scale. The freeboard R_c in our model tests was 0.05 to 0.35 m, and the water depth at the toe was $h = 0.65 \sim 0.95$ m. There is no need to test even larger R_c, since the overtopping will become negligible. The location of the cylinder with respect to the seawall's edge, x_c, was varied from 0.09 m ($1.5D$) to 0.53 m, to examine how the inline force changes with x_c. Note that the measured incident wave heights may not be exactly the same as the input value as shown in Table 1, but generally the actual value may be within $\pm 10\%$ range of the input value. The detailed test information can be found in Table S2 of the supplementary material.

3.4. Data analysis

In the wave flume experiments, a part of incoming wave energy is reflected by the seawall. Since our wave maker does not have the active-absorption function, the reflected waves are re-reflected by the wave maker towards the model, which is unrealistic and will contaminate the experimental results. Therefore, in the present study, our experimental results are only valid before the leading re-reflected wave reaches the seawall. The arrival times of the first mature wave and the first re-reflected wave at a given location in the flume were estimated using the wave celerity from linear-wave dispersion relationship. The time window of valid measurements was defined by the two arrival times. The maximum inline force and the maximum overtopping depth were obtained by averaging over the cycles in the time window. The free-surface elevation measurements from the two neighboring wave gauges (CG2 an CG3) within the selected time window were then used for separation of incident and reflected waves using the method of Goda and Suzuki (1976).

The measurements of water surface from the ultrasonic probes can be very

noisy when the water contains lots of air bubbles, e.g., the front of overtopping flow, so the noise was first removed using the outlier-removal function of MATLAB (i.e., the "rmoutliers" function). The force measurements contained some high-frequency noises produced mainly by the vibration of wave maker (note that most of noises are within the 20-30 Hz frequency band), so the raw measurements were filtered using a low-pass filter with a cut-off frequency of 10 Hz. Fig. 4 shows the processed data of an example case $S\_H20h20T25\_X9$ ($H = 20$ cm, $R_c = 20$ cm, T =2.5 s, $x_c = 9$ cm). In each subfigure, the two red lines indicate the time window of valid measurements.

4. Results and discussions

In this section, we first present some key experimental observations of overtopping process, providing a clear picture of the overtopping flow and the flow-cylinder interaction. We then present the experiment results of overtopping flow depth and force measurement and finally use them to calibrate the formulas for the maximum inline force presented in Section 2.

4.1. Overtopping process

Wave overtopping for a sloped seawall without an influencing foreshore starts with the wave breaking on the slope, which is characterized by the Iribarren number, I_r. For the present study, I_r varies between 1 and 4. A plunging-type breaker occurs for I_r smaller than 3 (Schüttrumpf and Oumeraci, 2005), so it should be the main breaker type for the waves considered in this study. For waves with I_r close to or larger than 3, the wave breaking should also have the feature of surging breaker. In our experiments,

indeed significant difference in wave breaking is observed between low- I_r (e.g., $I_r < 2$) and high- I_r (e.g., $I_r > 3$) cases.

We select two representative tests $S\_H16h85T15\_X09$ (H = 16 cm, R_c = 15 cm, T =1.5 s, x_c = 9 cm) and $S\_H16h85T30\_X09$ (only difference from the other case is that T = 3 s) and show the snapshots of their wave breaking process in Fig. 5, respectively. The short-period test has $I_r = 1.56$, so a typical plunging breaker occurs on the slope. The left column of Fig. 5 presents four snapshots from the moment when the plunging jet begins to impinge onto the slope (Fig. 5a-1) to the end of the wave run-up phase (Fig. 5a-4). The whole process takes about 0.76 s (or half of a wave period). At the beginning of impingement, the tip of the plunging jet just touches the seawall slope (Fig. 5a-1), and a big air pocket is trapped inside the flow. The impingement turns the plunging jet into a violent water splash, and the trapped air pocket collapses and evolves into a breaking roller (Fig. 5a-2). Subsequently, the water splash is organized into a runup jet along the seawall surface, which is highly aerated and has a very high speed (Fig. 5a-3). Air bubbles are distributed throughout the runup jet, so the flow appears 'white'. During this process, the breaking roller remains at the same location but continues to collapse till the end of wave breaking (Fig. 5a-4).

The wave breaking of the long-period test is presented in the right column of Fig. 5. This test has $I_r = 3.13$ close to the limit of 3.3, and the process indeed follows that of a surging breaker. Instead of having a significant plunging jet, only a tiny breaker occurs near the instantaneous waterline (as shown in Fig. 5b-1). This local breaking creates a thin and foamy runup jet which is pushed upslope by the main body of the wave crest. In Figs. 5b-1 to

5b-4, a substantial amount of water surges up the seawall slope in a rather peaceful manner, so the runup flow does not contain many air bubbles, which is very different from the plunging breaker. By comparing Figs. 5a-4 and 5b-4, it can be easily seen that a surging breaker (due to larger I_r) can produce a deeper wave runup flow than a plunging breaker.

The difference in wave breaking process leads to different behaviors of the overtopping flow. For plunging-type breaker, a thin and very foamy runup jet shoots out from the breaking roller, so when this jet crosses the seawall's edge and becomes overtopping flow, it can be very 'white' (i.e., highly aerated) and fast. For surging-type breaker, a layer of clean water surges up the slope in a peaceful manner, so the resulting overtopping flow appears 'greener' and slower than that produced by a plunging breaker. In Figs. 6a and 6c, the overtopping flow of two tests with the same wave height (H = 16 cm) and freeboard (R_c = 15 cm) but different wave periods (T = 2 s and T = 3 s) are presented. Obviously, the overtopping flow of the long-period test (I_r = 3.13, Fig. 6c) is a lot 'greener' than that of the short-period test (I_r = 2.08, Fig. 6a). Another factor controlling the aeration of overtopping flow is the relative freeboard, R_c/H. As the runup flow climbs up the seawall slope, the entrained air within the flow rises to the free surface and escapes. Thus, a larger R_c/H allows a longer runup traveling time and consequently reduces the aeration of the overtopping flow. The tests in Figs. 6b and 6d have the same wave conditions as the tests in Figs. 6a and 6c, but the R_c is increased to 25 cm. The overtopping flow with a larger R_c/H indeed appears 'greener'. These observations confirm the concept that the overtopping flow's behavior is controlled by the two dimensionless parameters, I_r and R_c/H.

Some key observations of the flow-cylinder interaction are presented here based on a typical test $S\_H16h85T30\_X09$. As shown in Fig. 7a, when the front of the overtopping flow strikes onto the cylinder, some water is diverted upward around the point of striking. The water continuously climbs up the cylinder until reaching the maximum runup level, which can be a few times of the overtopping flow depth, as shown in Fig. 7b. This runup flow develops and vanishes quickly. For example, it takes about 0.2 s for the maximum runup to occur for the selected test, and another 0.3 s for the runup flow to falls back into the main overtopping flow, while the whole overtopping process lasts 1.5 s. The runup flow along the cylinder is very thin (estimated to be a few mm thick in Fig. 7b), so it should not produce a substantial pressure on the cylinder. The runup height is determined by the kinematic energy of the incoming overtopping flow, so a larger runup height indicates a faster incoming flow. Note that the dynamic pressure of a jet flow hitting a solid surface is scaled with the incoming flow's kinematic energy, so a larger runup height also indicates a larger pressure (and hence larger inline force) on the cylinder's front surface. Due to the blockage of the cylinder, the overtopping water piles up in front of the cylinder, but a wake flow with a smaller water depth is developed behind the cylinder. This phenomenon can be well observed in Fig. 7c. The spatial variation of water depth around the cylinder will apparently lead to a net pressure force in the flow's direction.

4.2. Overtopping flow depth

4.2.1. Temporal variation

As mentioned in the last section, the Iribarren number, I_r, plays a key role in wave breaking and hence controls the behavior of overtopping flow.

Therefore, we present the overtopping flow depth for two tests with very different I_r values in Figs. 8a ($I_r = 3.46$) and 8b ($I_r = 1.73$). Both tests have the same wave height ($H = 13$ cm) and freeboard ($R_c = 15$ cm). In each subfigure, the flow depth measurements at three locations, i.e. $x = 0$ cm, $x = 18$ cm and $x = 54$ cm, are presented.

We first discuss the long-period test ($T = 3$ s) in Fig. 8a. Each overtopping event is represented by a hump in the time series. At the leading edge of the seawall ($x = 0$ cm, red solid line), the flow depth increases quickly with time within each overtopping event. The maximum flow depth $d_{0m} = 0.04$ m occurs at about 0.4 s since the arrival of the overtopping flow. The decrease of flow depth takes a longer time, e.g., a significant reduction of flow depth occurs within about 1 s after the moment of maximum flow depth. After the passing of the main overtopping flow, there is some residual water left on the seawall, which slowly flows back to the flume or into the overtopping tank, so in each overtopping event there is a 'long tail' of thin and slowly-decaying flow depth, e.g., $t = 41$ to 42 s in Fig. 8a. The time series is rather smooth and has one primary peak. This is because the overtopping flow is rather 'green' when a surging breaker occurs under a large I_r. Meanwhile, the overtopping flow is quite uniform in the spanwise direction, which also contributes to the smoothness of the measurement. For example, the front waterline of the overtopping flow is quite straight for the similar tests with $T = 3$ s in Figs. 6c and 6d. The flow depths at $x = 18$ cm and $x = 54$ cm are similar to that at the leading edge in terms of the temporal variation, but the maximum value decreases with x. For this test, the average d_{0m} is reduced to be about 0.02 m at $x = 54$ cm, which is about half of that at the

leading edge.

The short-period test (T = 1.5 s) is presented in Fig. 8b. Compared with the results in Fig. 8a, the smoothness of the measured time series is greatly reduced. For instance, there can be multiple peaks in each overtopping event. This is mainly because of the significant flow aeriation produced by the plunging-type breaker. The presence of air bubbles makes the water surface uneven. Also, the overtopping flow can also be quite 3-dimensional for tests with a low I_r value, since the origin of the overtopping flow, i.e., the water splash after the impingement of plunging jet, is very 3-dimensional. Nevertheless, it is still reasonable to say that the overall temporal variation of overtopping flow is similar to that of the long-period (or large I_r) test, i.e., a fast increase followed by a slow decrease. The maximum flow depth, d_{0m}, is about 0.012 m at the leading edge, and is reduced to about 0.006$\sim$0.008 m at x = 54 cm. Comparing to the long-period test (T = 3 s), the overtopping flow depth is found to be reduced by decreasing wave period, which agrees with the existing knowledge (see EurOtop 2018).

Although there is no direct velocity measurement, a representative velocity, V_{rep}, of the overtopping flow can be evaluated based on the lag of arrival time of the overtopping flow between two locations. In Fig. 8, the lag, Δt, between the onsets of overtopping event at x = 54 cm and x = 0 cm can be estimated. By dividing 54 cm with Δt, we obtain the V_{rep}, which is essentially an average velocity of the overtopping's front within the period of Δt. The two selected tests have similar value of Δt = 0.50 s, so the obtained V_{rep} is about 1 m/s for both tests. Overtopping flow velocity is believed to be proportional to overtopping flow depth (EurOtop 2018). Note that the

overtopping flow in the short-period test has a much smaller flow depth than that in the long-period test, so it is expected to have lower flow velocity, which does not agree with the obtained V_{rep}. In other words, the overtopping flow produced by plunging-type breaker is faster than that produced by a surging-type breaker, if the two flows have similar flow depth.

4.2.2. Maximum overtopping flow depth

The maximum overtopping flow depth at the leading edge, d_{0m}, is an important parameter, which determines the maximum inline force on a cylinder. To facilitate the comparisons among tests with different wave conditions and freeboard, we here considered the normalized maximum flow depth, i.e., d_{0m}/H. As discussed in the previous section, the behavior of overtopping flow is controlled by two dimensionless parameters, i.e., the Iribarren number, I_r, and the normalized freeboard, R_c/H. Thus, in Fig. 9, we plot d_{0m}/H against I_r and R_c/H. It can be clearly seen that d_{0m}/H increases with I_r and decreases with R_c/H. In other words, with a fixed wave height, the depth of the overtopping flow increases with flow period (larger period gives larger I_r) and decreases with the freeboard. For waves with a surging breaker (I_r close to 3), d_{0m}/H is between 0.5 and 0.2 for R_c/H between 0.5 and 2. For waves with a plunging breaker (I_r less than 2), d_{0m}/H is between 0.25 and 0.05 for R_c/H between 0.5 and 2. Scandoval (2016) analyzed 10 video footages from some Internet sources (e.g., YouTube), in which pedestrians lose balances under wave overtopping flows. He observed that the depth of overtopping flows in these videos are all below the knees of pedestrians, so the depth of a dangerous overtopping flow is of $\mathcal{O}$(10 cm). For a wave height of 1$\sim$2 m, the d_{0m}/H for a dangerous overtopping flow is of $\mathcal{O}(0.1)$, which is well within

the range of d_{0m}/H of our experiments. Therefore, some of our tests, if they are scaled up to field conditions, can indeed be dangerous.

The overtopping flow depth is commonly given by,

$$d_{0m} = \alpha(R_u - R_c) \tag{7}$$

where R_u is the wave runup and α is an empirical parameter usually obtained by fitting experimental results. Schüttrumpf and Oumeraci (2005) developed the following prediction equation of R_u, which can be directly applied for regular waves,

$$R_u = min\left(I_r, I_{r,tran}\right) H \tag{8}$$

where I_r is the Iribarren number and $I_{r,tran} = 3$ is the I_r at the transition of plunging and surging breaker (Schüttrumpf and Oumeraci, 2005). Combining Eq. (7) and Eq. (8), we get,

$$d_{0m} = \alpha H(min(I_r, 3)–R_c/H) \tag{9}$$

Van Gent (2003) obtained $\alpha = 0.15$ by fitting his irregular-wave experiments. Fig. 10 shows the comparison of measured and predicted d_{0m} using Eq. (9) and $\alpha = 0.15$. We can see that the data generally follow a linear trend, but the predicted d_{0m} (red dots) is about 30% less than measured value. A good fit is obtained by using $\alpha = 0.223$, with RMSE = 0.0073. The fitted coefficient is generally consistent with Van der Meer et al. (2012) and EurOtop (2018), who also found that $\alpha = 0.15$ is a bit small and they suggest that $\alpha = 0.20$ should be used for a slope = 1:3 and 1:4. Based on their measured flow depths (exceeded by 50% of the incident waves) at the leading edge of seawall crest (slope=1:4 and 1:6) due to irregular wave overtopping flow, Schüttrumpf and

Oumeraci (2005) obtained an empirical equation as,

$$d_{50\%} = 0.168 H_s (min(I_r, 3) – R_c/H_s) \tag{10}$$

The coefficient 0.223 obtained by fitting our data is larger than that in Eq. (10). Note that Eq. (10) is for $d_{50\%}$, but H_s is the average value of largest 1/3 of incident waves. If we change $d_{50\%}$ to $d_{1/3}$, the coefficient 0.168 should increase accordingly. This also indicates that our coefficient of 0.223 is reasonable.

4.2.3. Landward decay

As discussed in section 3.2, four ultrasonic sensors were deployed to measure the overtopping flow depths at four different locations shown in Fig. 3. From those measurements, we obtained local maximum overtopping flow depth d_m. To illustrate how the maximum overtopping flow depth decreases with the increasing distance to the seawall's leading edge (or landward decay), we present in Fig. 11 the normalized maximum flow depth $d_m(x)/d_{0m}$ with the location x, based on a set of 190 tests with different test conditions and x. Here the x-coordinate is normalized by d_{0m}, since d_{0m} is a characteristic length scale of the overtopping flow. As shown by the data cloud, $d_m(x)/d_{0m}$ rapidly decreases with x/d_{0m}, e.g., $d_m(x)/d_{0m}$ reaches about 0.5 for $x/d_{0m} = 25 \sim 35$. For a prototype d_{0m} of about 0.1∼0.2 m, it means that 50% reduction of flow depth occurs within 2∼7 m from the leading edge. We fit an exponential decay to the data cloud,

$$\frac{d_m(x)}{d_{0m}} = \exp\left[-0.104\left(\frac{x}{d_{0m}}\right)^{0.559}\right], 0 < \frac{x}{d_{0m}} < 45 \tag{11}$$

Eq. (11) is represented by the red solid line in Fig. 11, while the two dashed lines are the ±20% bounds. It can be seen that most of the data points

are within the ±20% bounds, so the fitting has a reasonable accuracy, with RMSE = 0.0788. The decay of overtopping flow depth is because the overtopping water collapses as it passes the leading edge of the seawall, which converts the flow's potential energy to kinematic energy. As a result, the overtopping flow accelerates shortly after entering the crest area. For our application (overtopping risk assessment), it is not necessary to understand $d_m(x)$ for very large x/d_{0m} (e.g., the width of the promenade may be only a few meters).

4.3. Inline force on the cylinder

4.3.1. Temporal variation

This section presents the inline (or horizontal) force on a cylinder due to the overtopping flow. Following Section 4.2, attention is paid to the effect of Iribarren number. The discussion is based on the same two cases shown in Fig. 8.

Fig. 12 presents the inline force on a cylinder located at $x_c = 9$ cm. In each sub-figure, the inline force is shown together with the overtopping flow depth at the seawall's edge. For the long-period test in which the overtopping flow is produced by a surging breaker, the temporal variation of the inline force is quite similar to that of the overtopping flow, as shown in Fig. 12a. For each overtopping event, the time series has a global peak between increase and a slow decrease. The maximum inline force occurs slightly earlier (by about 0.2 s on average) than the maximum flow depth. For the short-period test in which the overtopping flow is produced by a plunging breaker, the time series of the inline force appears irregular, similar to the time series of the overtopping flow depth, as can be seen in Fig. 12b. Within an overtopping event,

there can be multiple peaks of the inline force, and the measurement is much less periodic than that in Fig. 12a. This is not surprising, since the highly-aerated overtopping flow is very turbulent and 3-dimensional. Note that the cylinder was placed at the middle of the flume (1 m from the sidewalls), while the flow depth was measured at a different lateral location (0.7 m from one sidewall). Due to the 3-dimensionality of the flow, the measured flow depth does not necessarily occur near the cylinder, so the two measurements in Fig. 12b are not perfectly correlated as in Fig. 12a. Nevertheless, it can still be commented that the maximum inline force occurs before the maximum overtopping flow depth, and the inline force has a very sharp increase during the initial stage of flow-cylinder interaction.

4.3.2. Maximum inline force

We here present the calibration of the scaling parameters for the maximum inline force, i.e., C_H and C_d in Eqs. (4) and (6).

Since both C_H and C_d are functions of I_r and R_c/H, a large dataset is required to cover a reasonable parameter space. In this study, we limit the parameter space to $I_r \approx$[1.1, 3.5] and $R_c/H \approx$ [0.5, 2], which is applicable for most coastal revetments in Singapore.

There are totally 72 experiment tests. Using the information on F_{0m}, d_{0m}, H, D and β, the values of C_H and C_d were calculated. The variations of C_H and C_d with I_r and R_c/H are presented in the two subfigures of Fig. 13. Overall speaking, C_H is between 0.01 and 0.07. It increases with I_r but decreases with R_c/H, which reflects the ways that I_r and R_c/H influence the overtopping flow. C_d, however, decreases with I_r. This is because under the same flow depth, the overtopping flow produced by a plunging-type breaker

(low I_r) is faster than that produced by a surging-type breaker (large I_r). The value of C_d is about 1 for $I_r < 1.5$, but drops to 0.2$\sim$0.3 for $I_r > 3$.

Using the combined dataset of the experiment and numerical simulation in the accompanied paper (Chen et al., 2021), we developed a look-up table to quantify C_H (or C_d) values with the inputs of I_r and R_c/H (see the supplementary material for more details for the look-up table). To this end, the I_r-R_c/H domain is discretized into a uniform grid, i.e., I_r from 1.1 to 3.5 with an interval of 0.2 and the R_c/H from 0.5 to 2 with an interval of 0.1. The C_H and C_d values of the data points are interpolated linearly onto the grid, leading to the look-up tables. We also provide simple polynomial fits to the look-up table for easy use, but the fitting introduces additional error. More advanced data fitting methods (e.g., artificial neural network) may reduce the fitting error, but this is not the focus of this paper. Thus, in the following context we still use the look-up table for determining C_H or C_d. Here we want to highlight that the predictor is applicable for I_r between 1.1 and 3.5, R_c/H between 0.5 and 2, with $Rc/H >$(0.5I_r+0.75) not covered (the overtopping under such conditions is either extremely weak or prevented by a large freeboard).

We tested H-scaling formula (Eq. (4)) and d-scaling formula (Eq. (6)) , and the comparisons between predicted and measured values of F_{0m} for the experiment data are presented in Fig. 14. Using the H-scaling formula, the F_{0m} of 91.3% cases can be predicted with a relative error less than 30%, with RMSE = 0.363 N. For the d-scaling formula, also 91.3% of the cases have a relative error less than 30%, with RMSE = 0.344 N. Overall speaking, it can be commented that the accuracy of the two scaling laws is around $\pm$30%.

This is acceptable, considering that the cylinder is a surrogate of human body. Among the two, the H-scaling is recommended for engineering application, because it is more easy-to-use. the d-scaling requires the prediction of an intermediate variable, d_{0m}, which can be prone to some substantial errors. Note that F_{0m} is scaled with d^2, so 10% error of d would lead to a 20% error of F_{0m}.

4.3.3. Landward decay

To study the variation of the maximum inline force with the location of the cylinder, x_c, we placed the cylinder at 9, 15, 21, 39 and 53 cm from the actual leading edge and measured the inline force. To facilitate the comparisons among tests, we introduce a normalized maximum inline force, i.e., $F_m^* = F_m(x_c)/F_{0m}$, where $F_m(x_c)$ is the measured maximum inline force at x_c. We also introduce a normalized x-coordinate, i.e., $x^* = (x_c - x_{c0})/d_{0m}$, where d_{0m} is the maximum overtopping flow depth at the seawall's actual leading edge and x_{c0} is the leading edge defined for studying the inline force (x_{c0} = 9 cm in our experiments). As shown in Fig. 15, there is an overall trend that F_m^* decreases with x^*, and the decreasing rate reduces with x^*. In Fig. 15, the red solid line represents this formula (Eq. (12)), and the two red dashed lines denote 30% deviation from the red solid line. It can be seen that although the data scatter is quite large, most of the data points are within the two red dashed lines. This is partly because a large number of tests with plunging-type breakers are subject to quite large uncertainties, since the force measurement contains significant irregular fluctuations (as shown in Fig. 12). In principle, the decay rate should depend on the characteristics of overtopping flow and the ground friction on the seawall's crest, so $F_m^*(x^*)$

may vary with x^* in a complex manner. Nevertheless, as shown in Fig. 15, a simple exponential decay is fitted to the data cloud with a 30% inaccuracy, which gives

$$\frac{F_m(x)}{F_{0m}} = \exp\left[-0.059\left(\frac{x_c - x_{c0}}{d_{0m}}\right)^{0.66}\right], 0 < \frac{x_c - x_{c0}}{d_{0m}} < 45 \qquad (12)$$

Eq. (12) has RMSE = 0.158. The measurements suggest that it requires $x^* > 40{\sim}50$ to achieve a 50% reduction of maximum inline force. Note that a dangerous overtopping flow has a flow depth of 10∼20 cm, so it takes 4∼10 m from the leading edge for reducing 50% of the inline force. Such a long distance can possibly exceed the width of the seawall crest area. Based on this, it is reasonably to say that the decay of inline force with the distance to the leading edge is quite slow.

Note that Eq. (12) is purely based on laboratory experiments, in which the overtopping flow is largely 2-dimensional. In field conditions, the overtopping flow should be more 3-dimensional (e.g., the flow can spread out laterally). This should lead to a faster decay of overtopping flow, so it is expected that Eq. (12) underestimates the actual decay of inline force. This bias overestimates the risk and hence will add some conservatism in a risk assessment.

5. Experiment results of the tests using 3D-printed human model

In the previous sections, we used a cylinder as a surrogate of a human body. To check the validity of this simplification, some additional tests with 3D-printed human legs were conducted. Here we assumed a scenario that a pedestrian stand on the seawall crest with his legs slightly apart and faces

either forward or sideways, as shown in Fig. 16. We only consider the two legs of a pedestrian, because any overtopping flow that can fully submerge the whole lower body is surely dangerous. The width of the thigh of the leg model is 3 cm, so the total width of the model at the top is 6 cm, which is equal to the diameter of the cylinder used in the other tests. (see Fig. 16a and b). This allows us to study the equivalent diameter of a human body, i.e., the diameter of a cylinder that gives the same maximum inline force experienced by the 3D-printed model. The two legs in Fig. 16a were mounted to a perspex platform which is connected to the force transducer for force measurement. Note that there is a tiny gap between the foot bottom and the seawall crest to ensure that the model will not touch the ground during a test. Totally eight tests have been conducted, which cover two orientations of the model and four wave conditions (four different wave periods, T = 1.5, 2, 2.5, 3 s, but the same $H \approx 0.2$ m and $R_c = 0.15$ m). The wave conditions cover I_r from 1.46 to 2.89. We chose these test conditions because they give the largest maximum inline forces among our tests using a cylinder.

Figs. 17a to 17d show the time histories of the forces for a single cylinder ($D = 6$ cm), 3D-printed model facing forward and sideways to the overtopping flow for T = 1.5, 2, 2.5 and 3 s, respectively. It can be seen that for all four wave periods, the maximum force F_{0m} for a single cylinder ($D = 6$ cm) is always the largest, and the F_{0m} for 3D-printed model facing forward to the overtopping flow is the smallest. This is mainly because F_{0m} is proportional to the model's projected area in the flow direction. A single cylinder has the projected area of $D = 6$ cm times the overtopping flow depth. For the forward-facing 3D-printed model, the width of the projected area is only 6 cm

at the top (the thigh), but becomes smaller below the knees, e.g., the width of the ankle part is quite small (3.6 cm). By orienting the 3D printed model sideways-facing, the projected area in flow's direction is increased, mainly because the length of the foot is much larger than the width of the foot, but the total projected area is still smaller than that of the 6-cm-diameter cylinder. The magnitude of inline force can also be qualitatively assessed by checking the runup height of overtopping flow along the model. A larger runup is associated with more water being blocked by the model, so a larger inline force is applied on the model. Fig. 18 shows that for the same incident wave conditions ($H = 0.2$ m, $T = 1.5$ s) and the same freeboard ($R_c = 0.15$ m), runup height on the cylinder (6 cm) is the largest (≈ 13.5 cm) while that on 3D-printed model forward facing the flow is the smallest (≈ 8 cm), which is consistent with the force measurement. In terms of the temporal variation of the inline force, it is noted that the time series for the same group of tests are quite similar, as shown in Fig. 17.

To facilitate the comparisons among different tests, we calculate the ratio of the maximum inline force experienced by the 3D-printed model and by the cylinder model, i.e., $r = F_{0m\_3D}/F_{0m\_cyl}$. Table 2 presents the results. For the forward-facing 3D-printed model, the four tests have an average r of 0.50 with a standard deviation of $\pm 25\%$. For the sideways-facing 3D-printed model, the averaged r is increased to 0.70 ($\pm 25\%$). Therefore, a risk assessment should take the sideways-facing posture as the representative posture for pedestrians standing on the seawall. Of course, more details, e.g., the spacing between the legs and the shape of the shoe, may also play some roles, but we take these details as part of the overall model uncertainty.

The width of the human model is 6 cm (2 times the thigh width), and the maximum overtopping force is 70% of that experienced by a 6 cm-diameter cylinder. Note that the overtopping force is scaled with the diameter, so it can be concluded that the effective diameter of the human model is 70% $\times$ 6 = 4.2 cm, or 1.4 times the thigh width (3 cm). Thus, we suggest that the effective diameter of the human body is 1.4 times the width of the thigh.

6. A preliminary application of the formula

In Section 4, we developed two alternative formulae for estimating the inline force due to overtopping flow, and in Section 5 we further found that the equivalent diameter of a human body is 1.4 times the width of thigh. In this section, we present a preliminary application of the formula for safety assessment of pedestrians on the seawall crest and compare the results with the tolerable overtopping conditions in EurOtop (2018).

The essence of EurOtop's tolerable condition is that any overtopping event must not sweep off a pedestrian. Therefore, a maximum overtopping volume, V_{max}, of 600 l/m is proposed. The outcomes of this study allow us to conduct risk assessment based on whether the maximum inline force can move the pedestrian, so it is possible for us to further examine the threshold of V_{max} = 600 l/m in terms of the corresponding maximum inline force.

As shown in Fig. 19, we propose a simple case study for considering the stability of pedestrians on the seawall crest. A pedestrian is subjected to both inline force (here we only consider largest F_{0m}) due to overtopping flow and resistive force (f) due to ground friction. The pedestrian is assumed to be destabilized if $F_{0m}/f > 1$. The width of the human's thigh is assumed

to be $D_t = 15$ cm, so the equivalent cylinder diameter is $D = 21$ cm. W is the weight of an average adult of 60 kg, so $W = 588$ N. Note that the overtopping flow velocity is very large, thus the pedestrians can be flushed away when the flow depth is small (20∼40 cm). This flow depth is negligible compared with the normal height of a pedestrian (150∼180 cm). Therefore, the buoyancy force can be neglected. The ground friction is the body weight times a friction coefficient. The friction coefficient can vary within a wide range, depending on the material and roughness of the seawall surface and pedestrians' shoes. Endoh and Takahashi (1994) reported values of frictional coefficient μ_s from 0.38 for leather shoe on concrete surface covered by seaweed to 1.49 for rubber shoe on rough concrete surface. Martínez-Gomariz et al. (2016) reported that μ_s for various types of shoes on street (concrete) surface, which varies from 0.44 for flip-flops to 0.69 for flat-soled shoes. In view that it is impossible to obtain a prior knowledge of shoe condition in predictions, many researchers adopted a single value for μ_s and treat the variation of μ_s as model uncertainty. For example, $\mu_s = 0.5$ in Jonkman and Penning-Rowsell (2008), $\mu_s = 0.46$ in Milanesi et al. (2015) and $\mu_s = 0.4$ in Endoh and Takahashi (1994). We shall follow this simplification in this study, and take $\mu_s = 0.5$ in the following analysis. however, we need to highlight that the actual μ_s value depends on local seawall surface condition and the allowable overtopping condition should be sensitive to μ_s value. For instance, if we only consider the μ_s reported in the literatures (0.38 to 0.69), the mean value is about 0.5 and the standard deviation is about ±20%. The corresponding variation of the allowable overtopping volume will be about ±20%. If we further consider the ±25% standard deviation of $r = F_{0m\_3D}/F_{0m\_cyl}$, a

total standard deviation will be about ±50%.

Based on our experimental results, we find that the overtopping volume is proportional to d_{0m}^2, so we calibrated some simple formulas for the prediction of d_{0m} and V. The details are presented in Appendix A. Based on the H-scaling (Eq. (4)) for predicting F_{0m} and V=7.756d_{0m}^2 (Eq. (A.1)) for predicting V, we calculated the ratio of force F_{0m}/f and the overtopping volume V for various wave conditions and freeboard (H = 0.4∼1.2 m; T = 2∼6 s; R_c = 0.2∼1.5 m), then we plotted F_{0m}/f against V in Fig. 20. It can be seen that generally F_{0m}/f increases with V. The critical conditions, F_{0m}/f = 1 and V = 600 l/m, divide the domain into four quadrants (see the solid and the dashed lines in Fig. 20). If there is a perfect equivalency between the two thresholds, we expect to see all data points within the 1st and the 3rd quadrants. Indeed, most data points are within these two quadrants. There is no data point within the 4th quadrant ($F_{0m}/f > 1$ but $V < 600$ l/m), and a small amount of points within the 2nd quadrant ($F_{0m}/f < 1$ but $V >$ 600 l/m). This suggests that V = 600 l/m represents the critical condition that the maximum inline force due to the overtopping can sweep off a human body. The discrepancy (i.e., some points within the 2nd quadrant) implies that V = 600 l/m is more conservative than $F_{0m}/f = 1$.

The preliminary application confirms the validity of the threshold V_{max} = 600 l/m in EurOtop (2018). This, in turn, demonstrates that the research outcomes of our study can indeed provide meaningful results for practical applications. Despite the good agreement, it should be noted that results demonstrated in Fig. 20 are based on the assumption that $\mu_s = 0.5$ and r = 0.7. If we consider the variability (i.e., the standard deviation) of these two

parameters, the threshold value V will be subject to a standard deviation of $\pm 50\%$. If other factors such as various postures (various gap between two legs, sitting, even lying on the crest), pedestrian's body shape, pedestrian's response to the overtopping flow, pedestrian's health condition and softness of skin and clothes among others, the risk of overtopping flow striking down a pedestrian on a seawall crest should not be assessed in a deterministic but in a statistical approach, as reported in Franco et al. (1994) and Bellotti et al. (2005).

The present research outcome based on regular waves can be extended to irregular waves by assuming a wave-by-wave approach, which has been demonstrated in in an accompanied paper (Chen et al., 2021). For an irregular wave train with a very narrow spectrum, the largest wave height H_{max} can be estimated following the method in Battjes and Groenendijk (2000). Assuming the largest wave overtopping event is caused by the wave with the obtained H_{max} and peak wave period T_p, then R_c/H_{max} and I_r can be computed following the present research outcome by taking this wave event as regular wave. With the computed R_c/H_{max} and I_r, C_H and F_{0m} can be computed for the largest event and a preliminary risk assessment can be conducted by evaluating F_{0m}/f.

7. Conclusion

In the present study, wave overtopping flow striking a human body (represented by a cylinder) on the crest of seawall is investigated through a large set of scaled wave-flume experiments. For simplicity, we focus on a simple-sloped seawall without an influencing foreshore and assume normally incident

waves. The measured physical quantities include the free surface elevations in the flume, the overtopping flow depths on the seawall crest and the inline impact force on the cylinder. A high-speed camera was also deployed for recording the flow process.

The characteristics of the overtopping flow is mainly controlled by the Iribarren number (I_r). The incoming wave breaks on the seawall's slope, and the type of breaker can be either plunging (small I_r) or surging (large I_r). Subsequently, a jet-flow alike overtopping flow is produced. The overtopping flow produced by a plunging breaker is thinner, fast and whiter (more aerated) than that produced by a surging breaker. As the overtopping flow impinges onto the cylinder, a significant water runup along the cylinder frontal surface is observed, while a wake flow is developed behind the cylinder. This leads to an asymmetric pressure distribution around the cylinder, resulting in a net inline force. The temporal variation of the inline force generally follows that of the local flow depth, but the maximum inline force occurs slightly earlier than the maximum flow depth. Both maximum flow depth and maximum inline force decay with the distance to the leading edge of the seawall, and both decays can be reasonably described by an exponential function.

Two formulae are proposed for the maximum inline force on a cylinder located at the seawall's leading edge (F_{0m}). The H-scaling formula relates F_{0m} with the wave height (H), while the d-scaling formula relates F_{0m} with the maximum overtopping flow depth at the seawall's leading edge (d_{0m}). The scaling parameters, which are functions of I_r and relative freeboard (R_c/H), are calibrated based on the large dataset generated by our flume experiments.

The overall inaccuracy is about 30%, which is acceptable for risk assessment, since more model uncertainties can be introduced by other sources (e.g., the complexity of human body shape). The H-scaling is recommended for practical use as the wave heights are usually reported.

To confirm the validity of representing a human body as a cylinder, we performed comparative experiments, comparing the inline forces on a cylinder and 3D-printed human model. It is found that the temporal variation of inline force on the human model indeed is very similar to that on a cylinder. It is also found that the inline force is maximized if the lateral side of the human body faces the incoming overtopping flow (sideways facing). This is because the projected area in the flow's direction is larger for this facing angle. Based on the experimental results, it is recommended that the equivalent diameter of a human body is 1.4 times the width of the thigh.

To demonstrate the applicability of our formulae, a preliminary application was carried out to assess whether the overtopping flow due to periodic waves hitting a simple-sloped seawall can threat a pedestrian on the seawall crest. The overtopping is considered dangerous if it can produce an inline force exceeding the ground friction. The overtopping volume, V, was also calculated, allowing us to check our model outputs against the $V = 600$ l/m thresholds for tolerable overtopping proposed by EurOtop (2018). It is found that indeed most of our calculations agree with the $V = 600$ l/m threshold, i.e., dangerous overtopping is predicted for $V > 600$ l/m, but safe overtopping is predicted for $V < 600$ l/m. Only for some situations with long wave period, the overtopping flow is assessed to be safe even V is over 600 l/m. This is because long waves produce relatively peaceful overtopping flows that

can deliver a large overtopping volume.

The motivation of this study is that the tolerable overtopping condition in EurOtop (2018) is specified in a relatively vague manner. For example, the allowable mean discharge rate is 10∼20 l/m/s for significant wave height of 1 m. Using our force predictor, the tolerable overtopping condition can be determined more precisely.

We must acknowledge that there are some limitations in our present study. First, due to the limitations of our wave flume experiments, the research outcomes in the present study, are only applicable for normal incident wave overtopping at simple sloped seawalls with a slope close to 1:3. Also only fresh water and no wind conditions have been tested, which are different from real situations. Second, the water depth at the toe is assumed to be deep enough for neglecting the influence of foreshore on wave overtopping, so all waves are non-breaking before hitting the seawall's slope. Third, the roughness and permeability of the slope have not been considered. Fourth, the preliminary study using 3D printed human model may only be a very preliminary step if safety assessment needs to be conducted as other factors like pedestrians' body shape and postures, clothes and their response to overtopping flows may also affect the impact force. Indeed, considering all of these uncertainties, the risk assessment can only be conducted in a statistical rather than deterministic approach.

In addition, in the experiments, we do not have detailed measurements of the overtopping flow velocity and surface pressure on the cylinder, which prevents us from having a deeper understanding of the physical process. Thus, in an accompanied paper (Chen et al., 2021), the same topic is inves-

tigated through a RANS-based 3-dimensional numerical simulation. In the accompanied paper, the validated numerical model is used to generate more data points for calibrating the H-scaling for various seawall slopes (1:2, 1:3 and 1:4) typically seen in Singapore. Also the numerical model is used to verify the preliminary applications in the present paper, by comparison of the simulated peak inline force on a cylinder and the predictions using the H-scaling.

Acknowledgments

This work was supported by the Climate Resilience Study Funds (CRSF) through Building and Construction Authority (BCA) and Public Utilities Board (PUB) of Singapore. The Department of Civil and Environmental Engineering in National University of Singapore is acknowledged for allowing us to use the hydraulic laboratory.

References

Abt, S., Wittier, R., Taylor, A., Love, D., 1989. Human stability in a high flood hazard zone1. JAWRA Journal of the American Water Resources Association 25, 881–890.

Allsop, W., Bruce, T., Pearson, J., Alderson, J., Pullen, T., 2003. Violent wave overtopping at the coast, when are we safe? Proceedings of the fifth international conference on coastal mangement. Edited by R.G. Mclnnes. Brighton, UK. , 54–69.

Arrighi, C., Oumeraci, H., Castelli, F., 2017. Hydrodynamics of pedestrians' instability in floodwaters. Hydrology and Earth System Sciences 21, 515–531.

Battjes, J.A., Groenendijk, H.W., 2000. Wave height distributions on shallow foreshores. Coastal Engineering 40, 161–182.

Bellotti, G., Briganti, R., Franco, L., 2005. Analysis of perceived hazard from wave overtopping at the ostia harbour rubble mound breakwater: a pilot test. Proc. ICE Conference on Coastlines, Structures and Breakwaters. Edited by N. W. H. Allsop. London, UK , 231–239.

Chen, H., Yuan, J., Cao, D., Liu, P., 2021. Wave overtopping flow striking a human body on the crest of a sloped seawall. part ii: numerical modeling. Coastal Engineering. Unpublished .

Chen, X., Hofland, B., Altomare, C., Suzuki, T., Uijttewaal, W., 2015. Forces on a vertical wall on a dike crest due to overtopping flow. Coastal Engineering 95, 94–104.

De Rouck, J., Van Doorslaer, K., Versluys, T., Ramachandran, K., Schimmels, S., kudella, M., Trouw, K., 2012. Full scale impact tests of an overtopping bore on a vertical wall in the large wave flume (gwk) in hannover. Proceedings of 33rd international conference on coastal engineering. Edited by P. Lynett. Santander, Spain , 1–13.

Endoh, K., Takahashi, S., 1994. Numerically modeling personnel danger on a promenade breakwater due to overtopping waves. Proceedings of 24th

International Conference on Coastal Engineering. Edited by Billy L. Edge. Kobe, Japan , 1016–1029.

EurOtop, 2018. Manual on wave overtopping of sea defences and related structures. an overtopping manual largely based on european research, but for worldwide application. Van der Meer, J. W. and Allsop, N. W. H. and Bruce, T. and De Rouck, J. and Kortenhaus, A. and Pullen, T. and Schüttrumpf, H. and Troch, P. and Zanuttigh, B. .

Foster, D.N., Cox, R., 1973. Stability of children on roads used as floodways : preliminary study. Manly Vale, N.S.W., University of New South Wales, Water Research Laboratory .

Franco, L., de Gerloni, M., van der Meer, J., 1994. Wave overtopping on vertical and composite breakwaters. Proceedings of 24th International Conference on Coastal Enegineering. Edited by Billy L. Edge. Kobe, Japan , 1030–1045.

Goda, Y., 2009. Derivation of unified wave overtopping formulas for seawalls with smooth, impermeable surfaces based on selected clash datasets. Coastal Engineering 56, 385–399.

Goda, Y., Suzuki, Y., 1976. Estimation of incident and reflected waves in random wave experiments. Proceedings of 15th International Conference on Coastal Engineering Edited by American Society of Civil Engineers. Honolulu, Hawaii, USA , 828–845.

Higuera, P., Lara, J.L., Losada, I.J., 2013. Simulating coastal engineering processes with openfoam®. Coastal Engineering 71, 119–134.

Higuera, P., Lara, J.L., Losada, I.J., 2014. Three-dimensional interaction of waves and porous coastal structures using openfoam®. part i: Formulation and validation. Coastal Engineering 83, 243–258.

Hughes, S.A., Thornton, C.I., 2016. Estimation of time-varying discharge and cumulative volume in individual overtopping waves. Coastal Engineering 117, 191–204.

Jonkman, S., Penning-Rowsell, E., 2008. Human instability in flood flows. JAWRA Journal of the American Water Resources Association 44, 1208–1218.

Lind, N., Hartford, D., Assaf, H., 2004. Hydrodynamic models of human stability in a flood. JAWRA Journal of the American Water Resources Association 40, 89–96.

Mares-Nasarre, P., Argente, G., Gómez-Martín, M.E., Medina, J.R., 2019. Overtopping layer thickness and overtopping flow velocity on mound breakwaters. Coastal Engineering 154, 103561.

Martínez-Gomariz, E., Gómez, M., Russo, B., 2016. Experimental study of the stability of pedestrians exposed to urban pluvial flooding. Natural Hazards 82, 1259–1278.

Van der Meer, J., Provoost, Y., Steendam, G.J., 2012. The wave run-up simulator, theory and first pilot test. Proceedings of 33th International Conference on Coastal Engineering. Edited by Lynett, P.. Santander, Spain , structures.65.

Van der Meer, J.W., Hardeman, B., Steendam, G.J., Schuttrumpf, H., Verheij, H., 2011. Flow depths and velocities at crest and landward slope of a dike, in theory and with the wave overtopping simulator. Proceedings of 32nd International Conference on Coastal Engineering. Edited by Jane McKee Smith and Patrick Lynett. Shanghai, China 1.

Milanesi, L., Pilotti, M., Ranzi, R., 2015. A conceptual model of people's vulnerability to floods. Water Resources Research 51, 182–197.

Molines, J., Herrera, M.P., Gómez-Martín, M.E., Medina, J.R., 2019. Distribution of individual wave overtopping volumes on mound breakwaters. Coastal Engineering 149, 15–27.

Nørgaard, J.Q.H., Lykke Andersen, T., Burcharth, H.F., 2014. Distribution of individual wave overtopping volumes in shallow water wave conditions. Coastal Engineering 83, 15–23.

Pan, Y., Kuang, C., Li, L., Amini, F., 2015. Full-scale laboratory study on distribution of individual wave overtopping volumes over a levee under negative freeboard. Coastal Engineering 97, 11–20.

Salauddin, M., Pearson, J., 2019. Wave overtopping and toe scouring at a plain vertical seawall with shingle foreshore: A physical model study. Ocean Engineering 171, 286–299.

Scandoval, C., 2016. Direct personnel hazard in wave overtopping flows at seadikes. Master's thesis. The University of Edinburgh. Edinburgh, United Kingdom.

Schüttrumpf, H., Oumeraci, H., 2005. Layer thicknesses and velocities of wave overtopping flow at seadikes. Coastal Engineering 52, 473–495.

Van Bergeijk, V.M., Warmink, J.J., Van Gent, M.R., Hulscher, S.J., 2019. An analytical model of wave overtopping flow velocities on dike crests and landward slopes. Coastal Engineering 149, 28–38.

Van Doorslaer, K., De Rouck, J., Audenaert, S., Duquet, V., 2015. Crest modifications to reduce wave overtopping of non-breaking waves over a smooth dike slope. Coastal Engineering 101, 69–88.

Van Gent, M.R.A., 2003. Wave overtopping events at dikes. Proceedings of 28th International Conference on Coastal Engineering. Edited by Jane McKee Smith. Cardiff, Wales , 2203–2215.

Nomenclature

β the slope of the sloped seawall. Unit: -

Δt time interval. Unit: s

μ_s the frictional coefficient. Unit: -

ν the fluid kinematic viscosity. Unit: m^2/s

π_1 dimensionless parameter. Unit: -

π_2 dimensionless parameter. Unit: -

π_3 dimensionless parameter. Unit: -

π_4 dimensionless parameter. Unit: -

π_5 dimensionless parameter. Unit: -

π_6 dimensionless parameter. Unit: -

ρ the fluid density. Unit: kg/m^3

C_d d-scaling coefficient. Unit: -

C_H H-scaling coefficient. Unit: -

D the cylinder diameter. Unit: m

$d_m(x)$ the maximum overtopping flow depth at x from the leading edge of the seawall crest. Unit: m

D_t the thigh diameter of the 3D printed human model. Unit: m

d_{0m} the maximum overtopping flow depth at $x = 0$ m from the leading edge of the seawall crest. Unit: m

f resistive force. Unit: $kg \cdot m/s^2$

F^* maximum inline force per unit cylinder diameter, i.e., $F^* = F_{0m}/D$. Unit: kg/s^2

F_m^* the normalized maximum inline force, F_m^*=$F_m(x_c)/F_{0m}$. Unit: -

$F_m(x_c)$ the measured maximum inline force at x_c. Unit: $kg \cdot m/s^2$

F_{0m} the maximum inline force (which is the overtopping striking force in the overtopping flow direction) at x_{c0}=$1.5D$. Unit: $kg \cdot m/s^2$

f_{d0m} function of d_{0m}. Unit: -

f_{F0m} function of F_{0m}. Unit: -

g the gravitational acceleration. Unit: m/s^2

H the wave height. Unit: m

h the water depth. Unit: m

H_{max} maximum wave height in an irregular wave train. Unit: m

I_r Iribarren number, $I_r = \tan\beta/\sqrt{H/L_0}$. Unit: -

L_0 deep water wavelength. Unit: m

M overtopping flow momentum flux. Unit: m^3/s

r the ratio of the maximum inline force experienced by the 3D-printed model and by the cylinder model, i.e., $r = F_{0m\_3D}/F_{0m\_cyl}$. Unit: m

R_c the freeboard of the sloped seawall. Unit: m

T the wave period of regular waves. Unit: s

t time. Unit: s

T_p the peak period of irregular waves. Unit: s

u the overtopping flow velocity. Unit: m/s

V overtopping volume for regular waves. Unit: m^3

V_{max} maximum overtopping volume for an irregular wave train. Unit: m^3

V_{rep} representative velocity. Unit: m/s

X the streamwise distance from the wave maker, i.e., $X = 0$ is the location of the wave maker. Unit: m

x the streamwise distance of ultrasonic sensor from the leading edge of seawall crest. Unit: m

x^* normalized x-coordinate, $x^* = (x_c - x_{c0})/d_{0m}$. Unit: -

x_c the streamwise distance of cylinder centre from the leading edge of seawall crest. Unit: m

x_{c0} the defined edge as 1.5 times cylinder diameter D from the actual leading edge, i.e., $x_{c0} = 1.5D$, where $x = 0$ is the actual leading edge. Unit: m

Figure captions

Figure 1: A typical sloped seawall in Singapore.

Figure 2: Definition of physical quantities related to F_{0m}.

Figure 3: Sketches of the experimental setup in (a) front view; (b) top view; (c) photo of the seawall; (d) cylinder and force sensor; (e) the whole wave flume.

Figure 4: Measurements for test $S\_H20h20T25\_X9$: (a) wave gauge 1 at $x = 6.65$ m ($x = 0$ is wave paddle), (b) wave gauge 2 at $x = 17.29$ m, (c) wave gauge 3 at $x = 17.83$ m, (d) wave gauge 4 at $x = 23.57$ m, (e) ultrasonic sensor 1 at the leading edge of seawall, (f) inline force on the cylinder.

Figure 5: Snapshots of wave breaking process for test $S\_H16h85T15\_X09$ (left column) and $S\_H16h85T30\_X09$ (right-column) over the sloped seawall. See the detailed descriptions for each sub-figure in the corresponding text.

Figure 6: Snapshots of overtopping flows. All snapshots are taken when the front of the overtopping flow reaches roughly 20 cm from leading edge of the seawall crest.

Figure 7: Snapshots of flow-cylinder interaction process for test $S\_H16h85T30\_X09$. The time sequence is (a)→(b)→(c).

Figure 8: Time series of overtopping flow depth for test $S\_H13h85T30$ ($H = 13$ cm, $R_c = 15$ cm, $T = 3.0$ s) and test $S\_H13h85T15$ ($H = 13$ cm, $R_c = 15$ cm, $T = 1.5$ s). For each test, we present a two-cycle cut.

Figure 9: Normalized maximum overtopping flow depth at the seawall's leading edge ($x = 0$ cm).

Figure 10: Comparison of predicted and measured d_{0m}.

Figure 11: Variation of maximum overtopping flow depth with the loca-

tion on the seawall crest.

Figure 12: Time series of inline force on the cylinder at $x_c = 9$ cm edge for two representative revetment tests.

Figure 13: Scaling parameters: (a) C_d; and (b) C_H.

Figure 14: Performance of the formulae for F_{0m}. The solid line indicates perfect agreement. The dashed lines indicate $\pm 30\%$ relative error.

Figure 15: Variation of maximum inline force with the location on the seawall crest.

Figure 16:(a) 3D-printed human leg model; (b) comparison with single cylinder model; Installation of the human leg model on the seawall crest: (c) forward facing the flow; (d) sideways facing the flow.

Figure 17: Typical time series of force for: single cylinder with $D = 6$ cm (black solid line); sideways-facing 3D-printed human model (90°, blue dash-dotted line); forward-facing 3D-printed human model (0°, red dashed line). $H = 0.2$ m, $R_c = 0.15$ m for all the tests.

Figure 18: Snap shots of the moment when runup of overtopping flow on the object reaches maximum (yellow dashed line indicates the top of runup): (a) a single cylinder with D= 6 cm; 3D-printed model (b) facing the overtopping flow; (c) perpendicular to overtopping flow.

Figure 19: Sketch of a simple model for human instability.

Figure 20: F_{0m}/f plotted against overtopping volume V.

Figure A1: Overtopping volume plotted against d_{0m}^2.

Table 1: Test conditions

h [m]	R_c [m]	H [m]	T [s]	x_c [m]	I_r
0.65∼0.95	0.05∼0.35	0.069∼0.209	1.2∼3	0.09∼0.53	1.33∼4.04

Table 2: Summary of the force ratio $F_{0m\_cyl}/F_{0m\_3D\_0°}$ and $F_{0m\_cyl}/F_{0m\_3D\_90°}$

Test ID	$F_{0m\_cyl}/F_{0m\_3D\_0°}$	Test ID	$F_{0m\_cyl}/F_{0m\_3D\_90°}$
$S\_H20h860T15\_3Dmodel$	2.03	$S\_H20h860T15\_3Dmodel\_90°$	1.23
$S\_H20h860T2\_3Dmodel$	2.27	$S\_H20h860T2\_3Dmodel\_90°$	1.45
$S\_H20h860T25\_3Dmodel$	2.26	$S\_H20h860T25\_3Dmodel\_90°$	1.78
$S\_H20h860T3\_3Dmodel$	1.51	$S\_H20h860T3\_3Dmodel\_90°$	1.25
Mean (Standard deviation)	2.02 (±0.36)	Mean (Standard deviation)	1.43 (±0.26)

Figure 1:

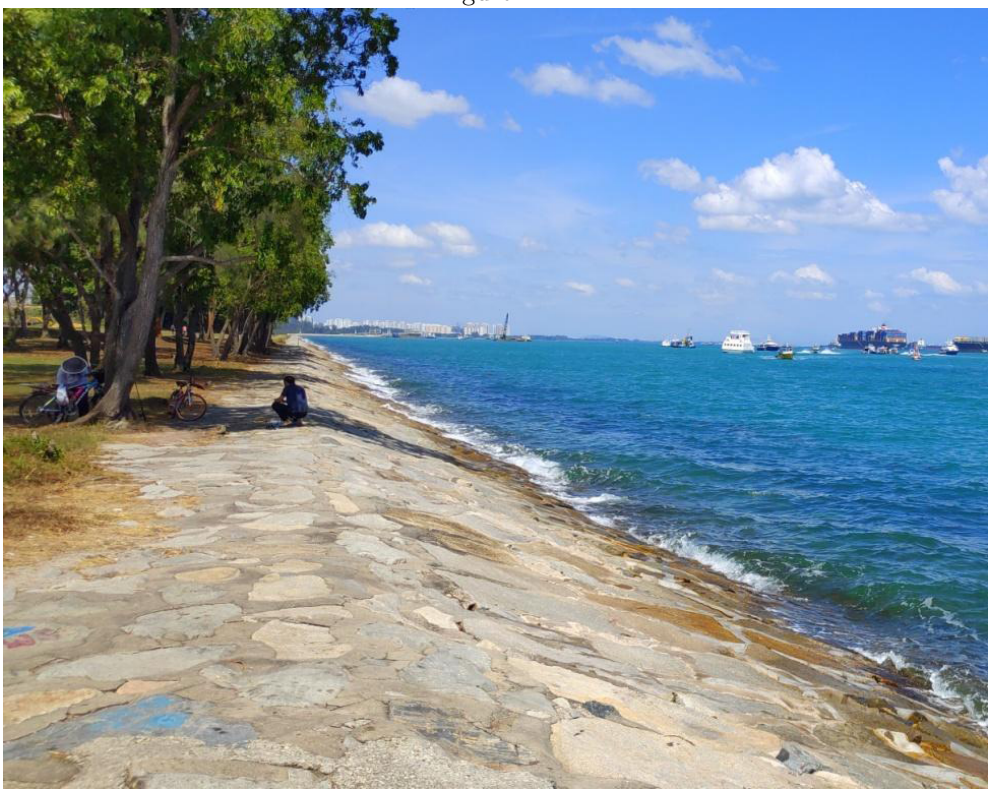

Figure 2:

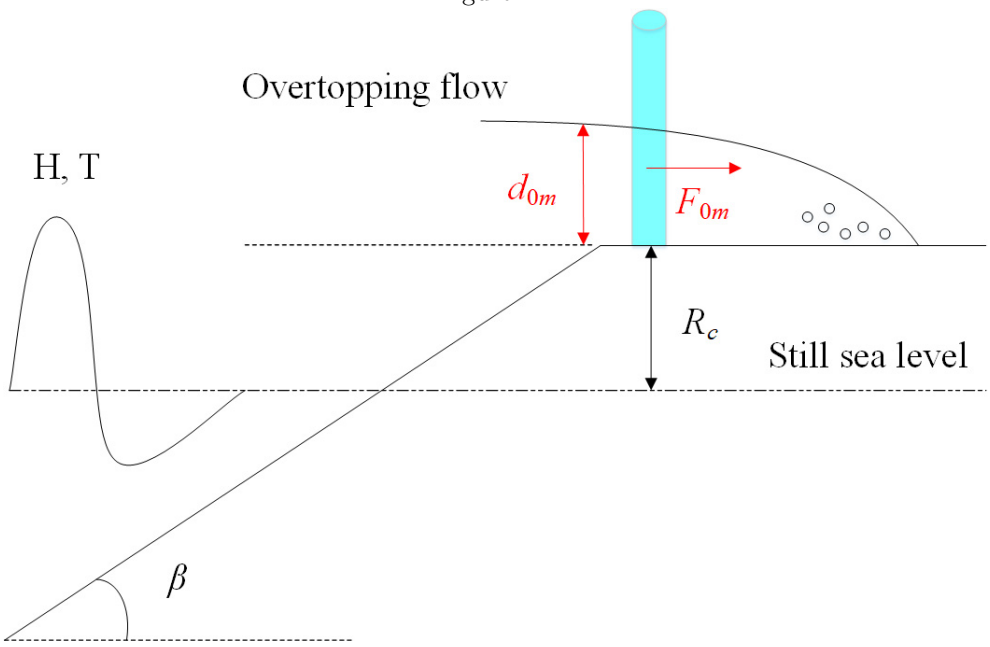

Figure 3:

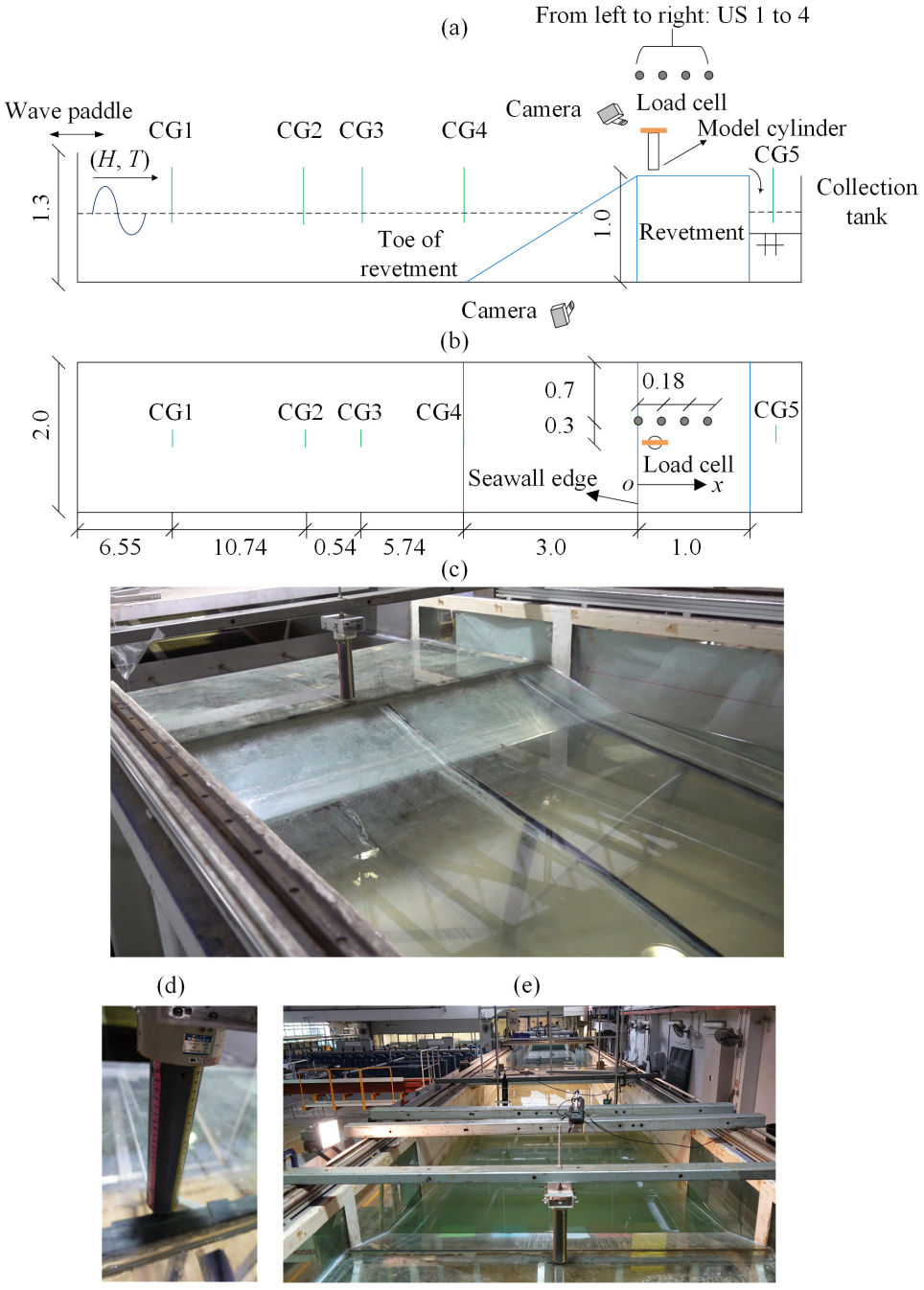
(a)
From left to right: US 1 to 4
Wave paddle
CG1
CG2
CG3
CG4
Camera
Load cell
Model cylinder
CG5
Collection tank
(H, T)
1.3
1.0
Toe of revetment
Revetment
Camera
(b)
2.0
CG1
CG2
CG3
CG4
0.7
0.3
0.18
CG5
Load cell
Seawall edge
o
x
6.55
10.74
0.54
5.74
3.0
1.0
(c)
(d)
(e)

Figure 4:

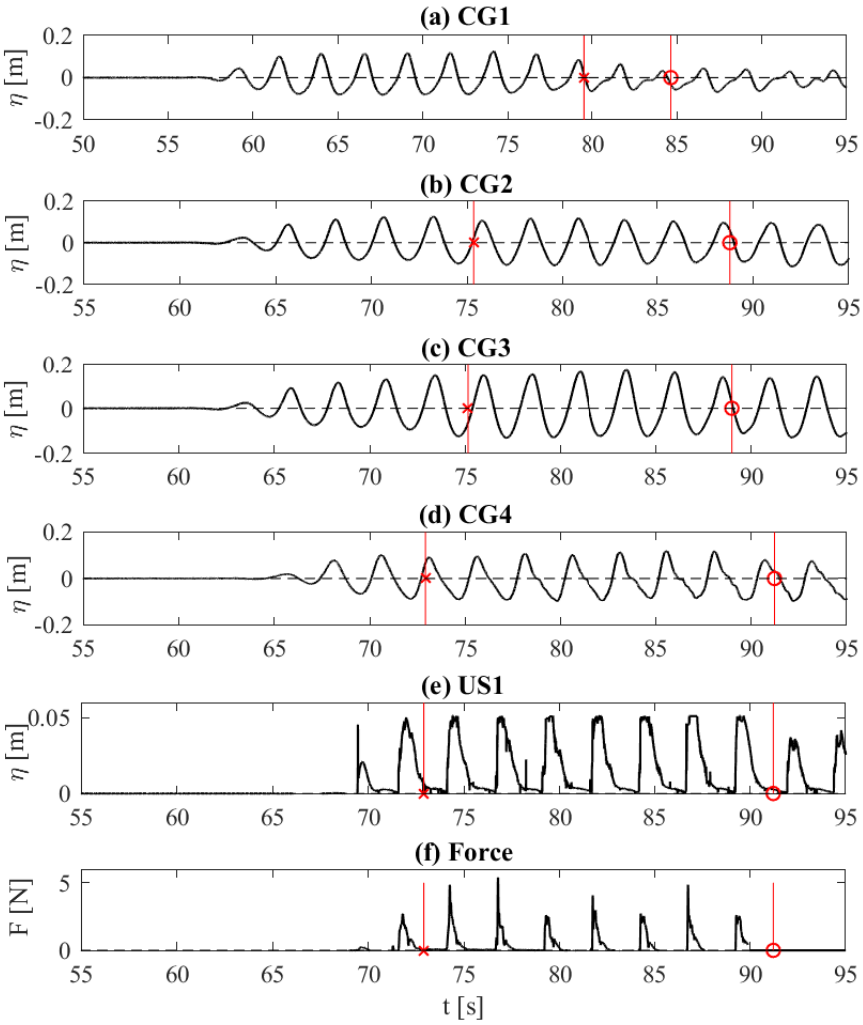

Figure 5:

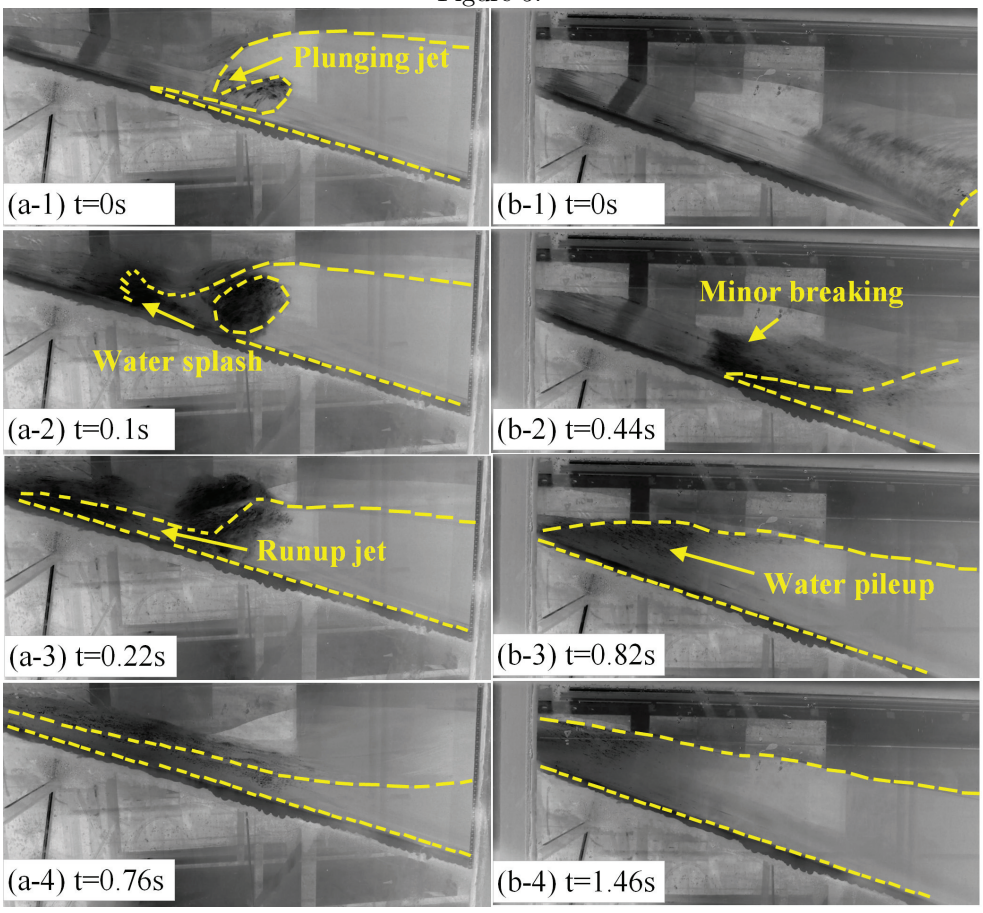
Plunging jet
(a-1) t=0s
(b-1) t=0s
Water splash
(a-2) t=0.1s
Minor breaking
(b-2) t=0.44s
Runup jet
(a-3) t=0.22s
Water pileup
(b-3) t=0.82s
(a-4) t=0.76s
(b-4) t=1.46s

Figure 6:

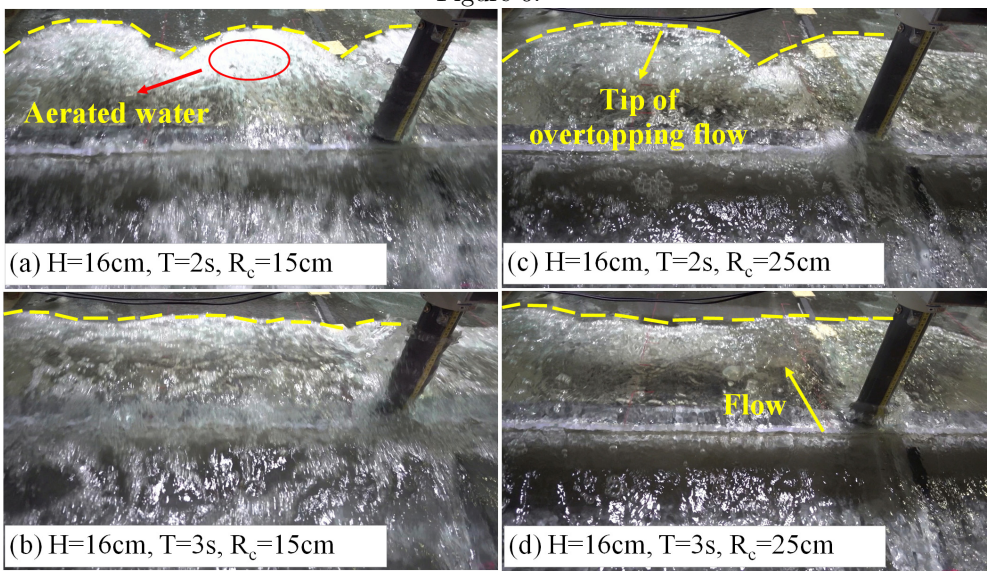

Figure 7:

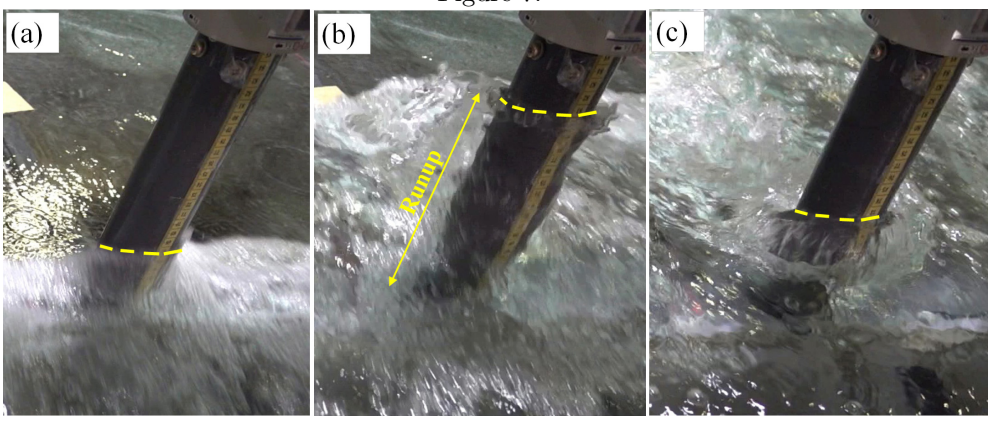

Figure 8:

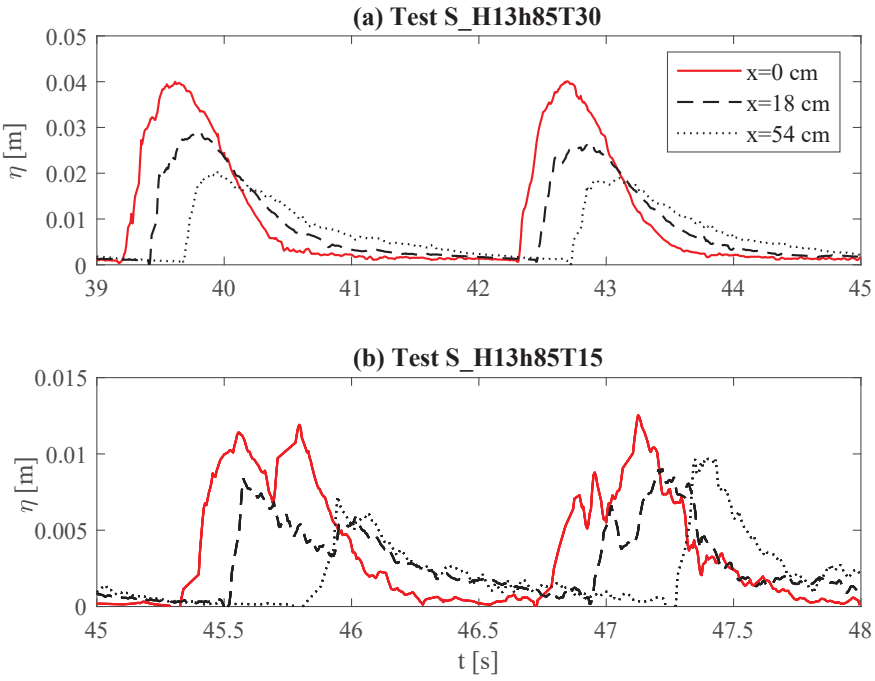
(a) Test S_H13h85T30
x=0 cm
x=18 cm
x=54 cm
η [m]
0.05
0.04
0.03
0.02
0.01
0
39
40
41
42
43
44
45
(b) Test S_H13h85T15
η [m]
0.015
0.01
0.005
0
45
45.5
46
46.5
47
47.5
48
t [s]

Figure 9:

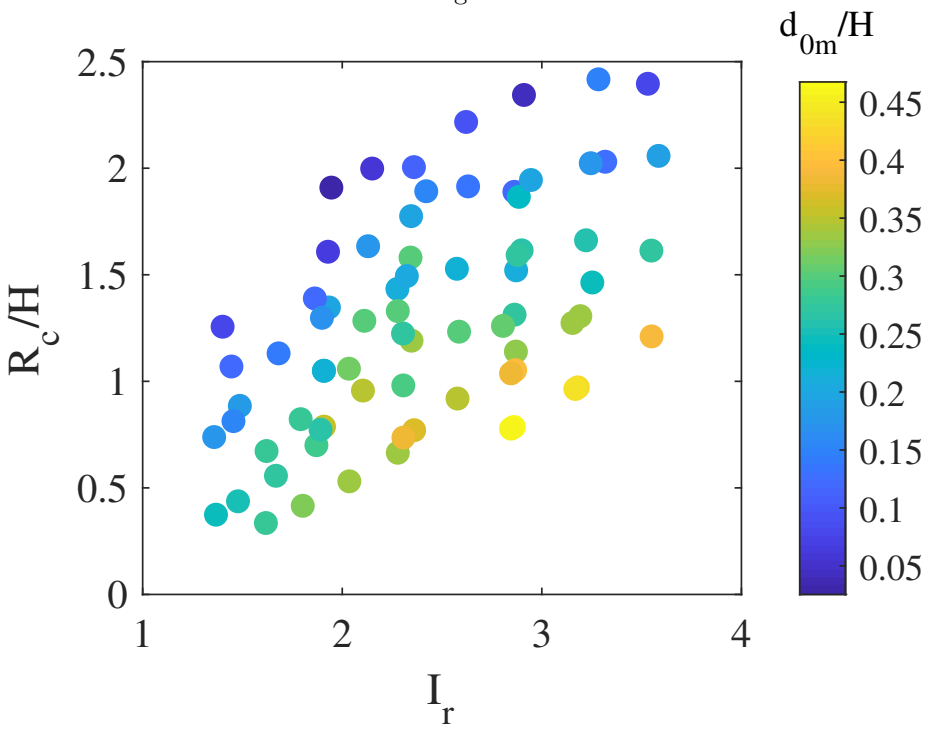

Figure 10:

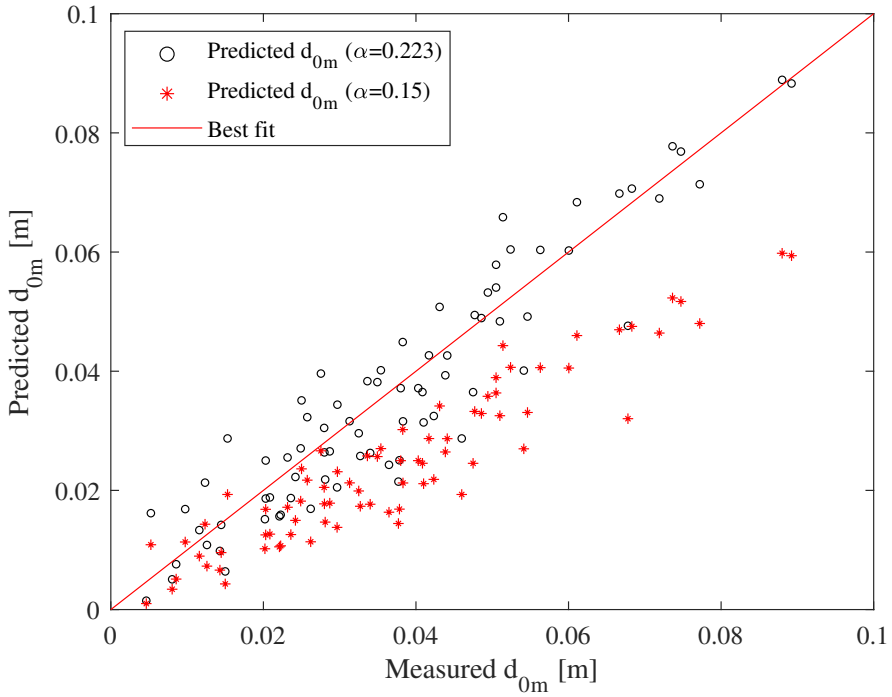
Predicted d0m (α=0.223)
Predicted d0m (α=0.15)
Best fit
Predicted d0m [m]
Measured d0m [m]
0
0.02
0.04
0.06
0.08
0.1

Figure 11:

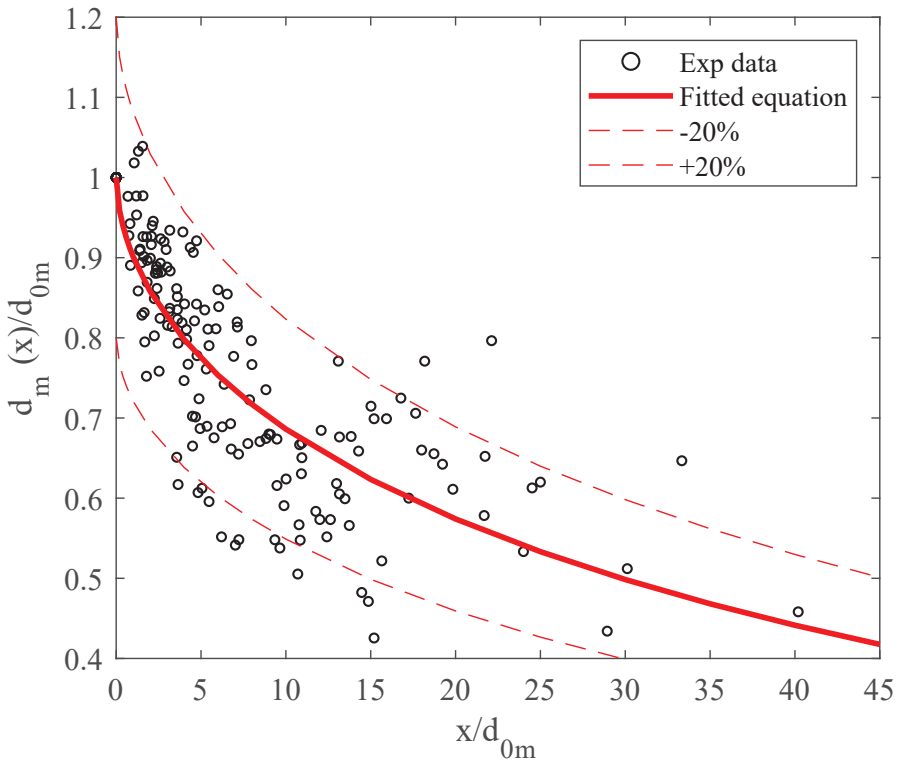
Exp data
Fitted equation
-20%
+20%
1.2
1.1
1
0.9
0.8
0.7
0.6
0.5
0.4
0
5
10
15
20
25
30
35
40
45
d m (x)/d 0m
x/d 0m

Figure 12:

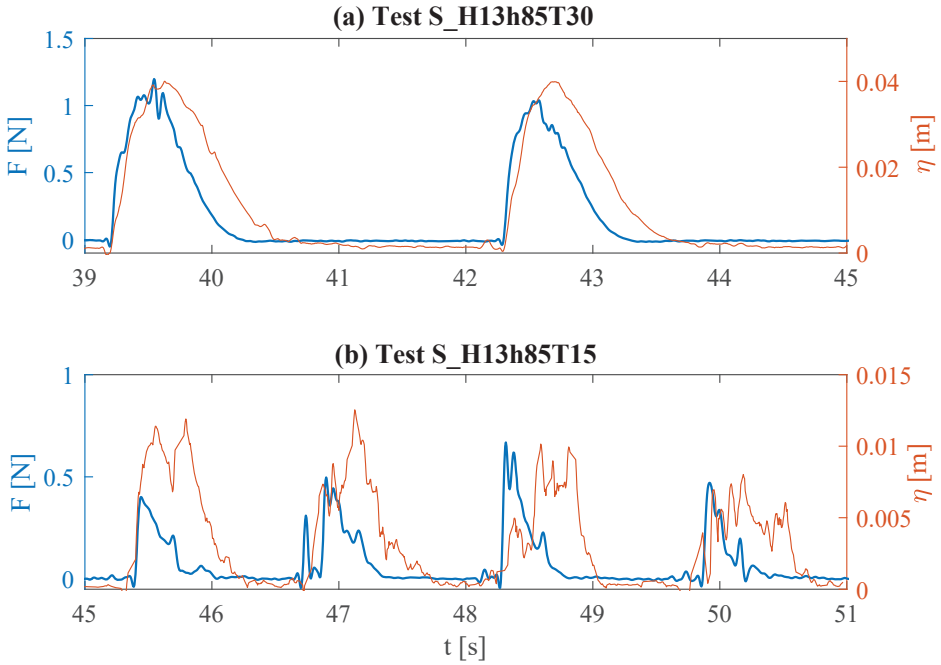

Figure 13:

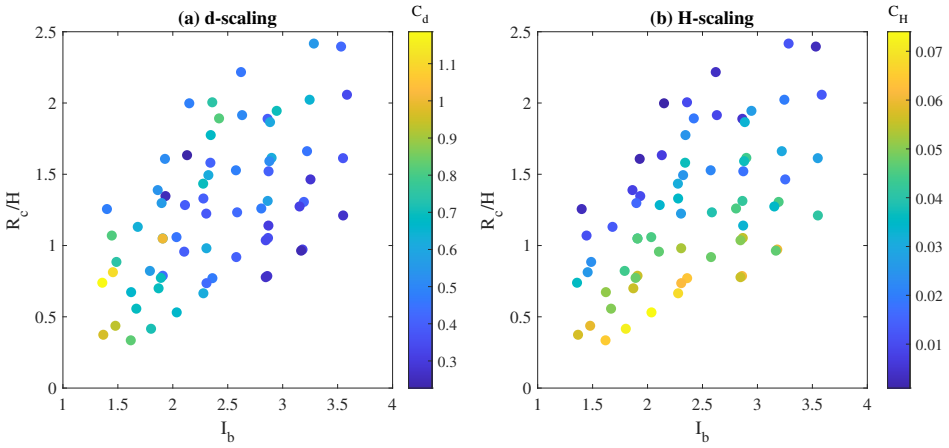

Figure 14:

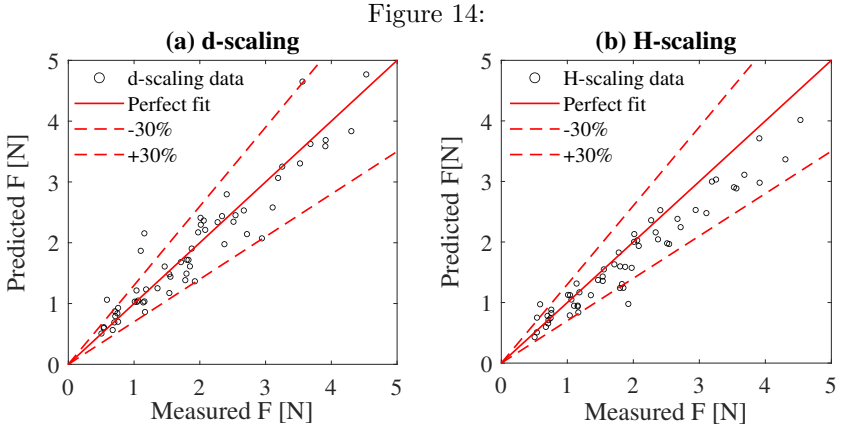
(a) d-scaling
d-scaling data
Perfect fit
-30%
+30%
Predicted F [N]
Measured F [N]
(b) H-scaling
H-scaling data
Perfect fit
-30%
+30%
Predicted F[N]
Measured F [N]

Figure 15:

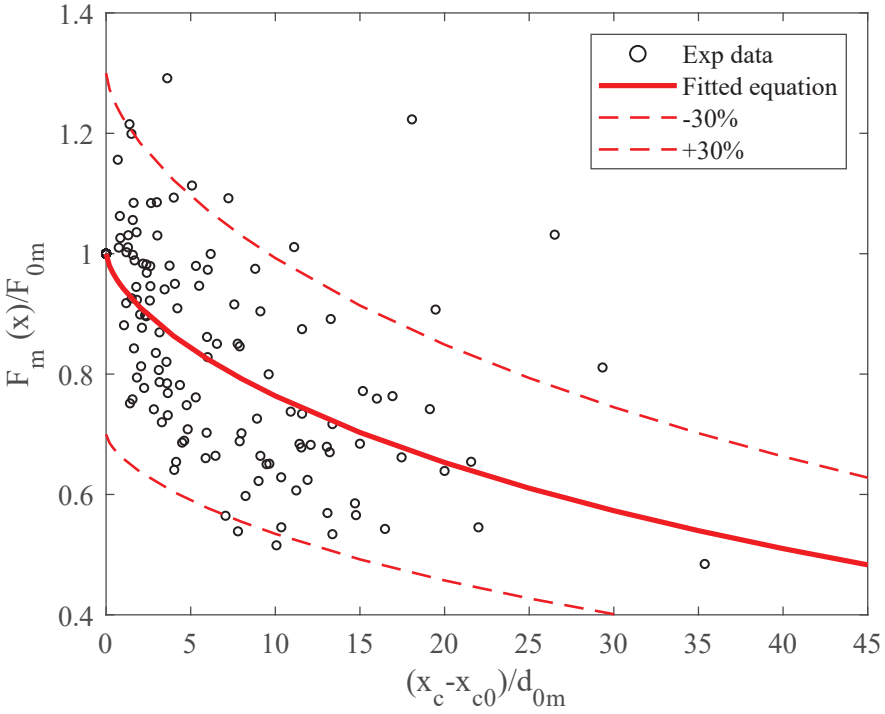
Exp data
Fitted equation
-30%
+30%
1.4
1.2
1
0.8
0.6
0.4
0
5
10
15
20
25
30
35
40
45
$F_m(x)/F_{0m}$
$(x_c-x_{c0})/d_{0m}$

Figure 16:

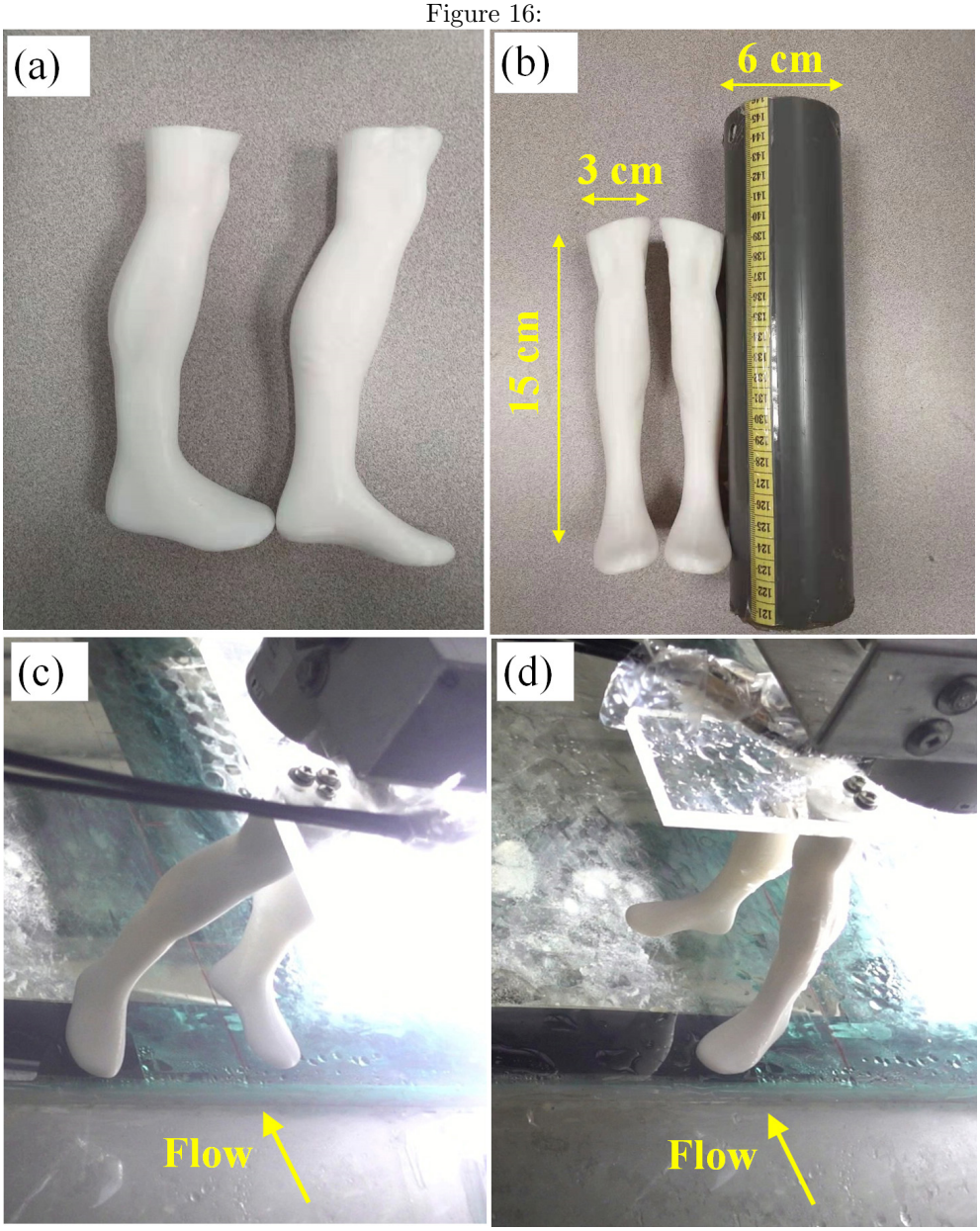

Figure 17:

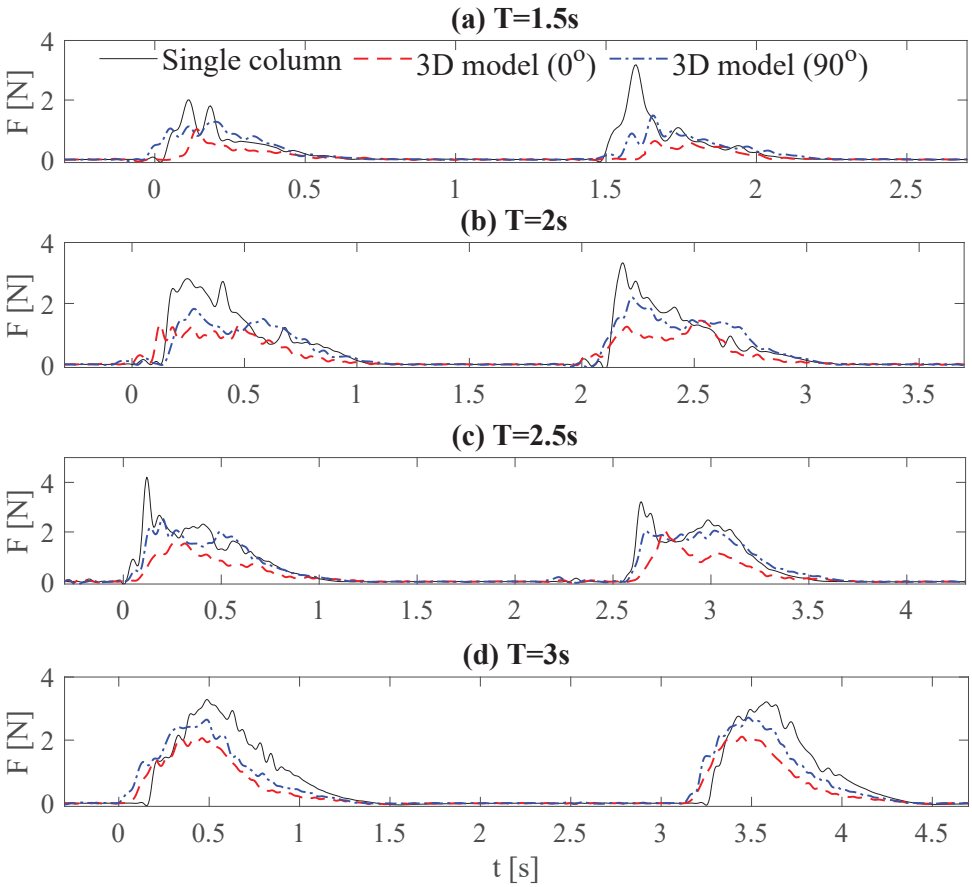

Figure 18:

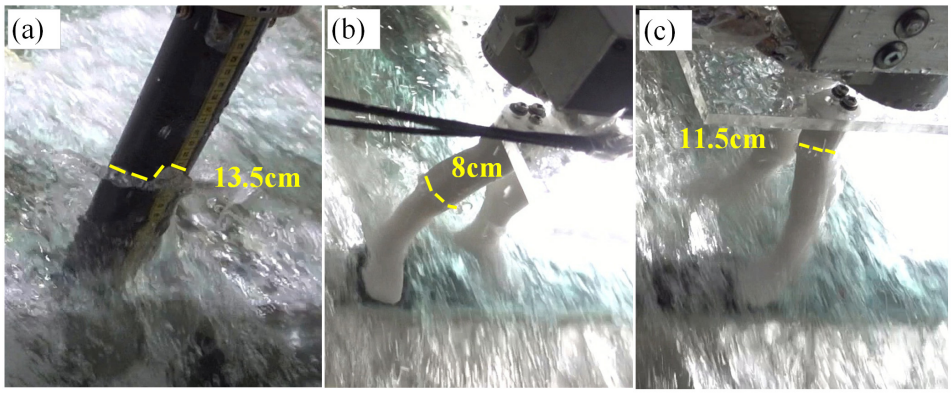

Figure 19:

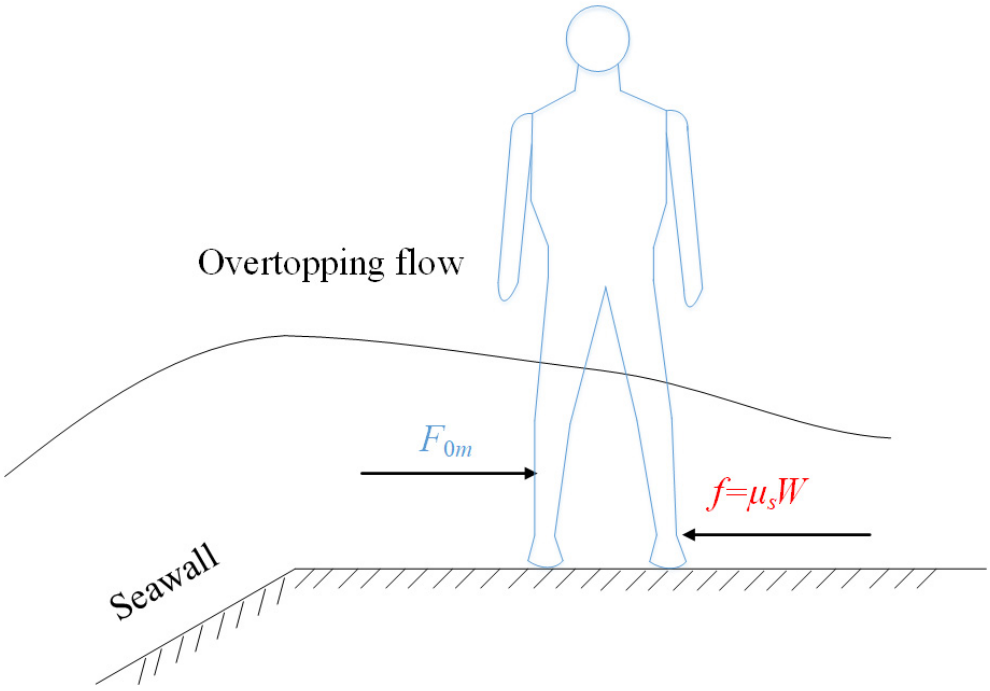

Figure 20:

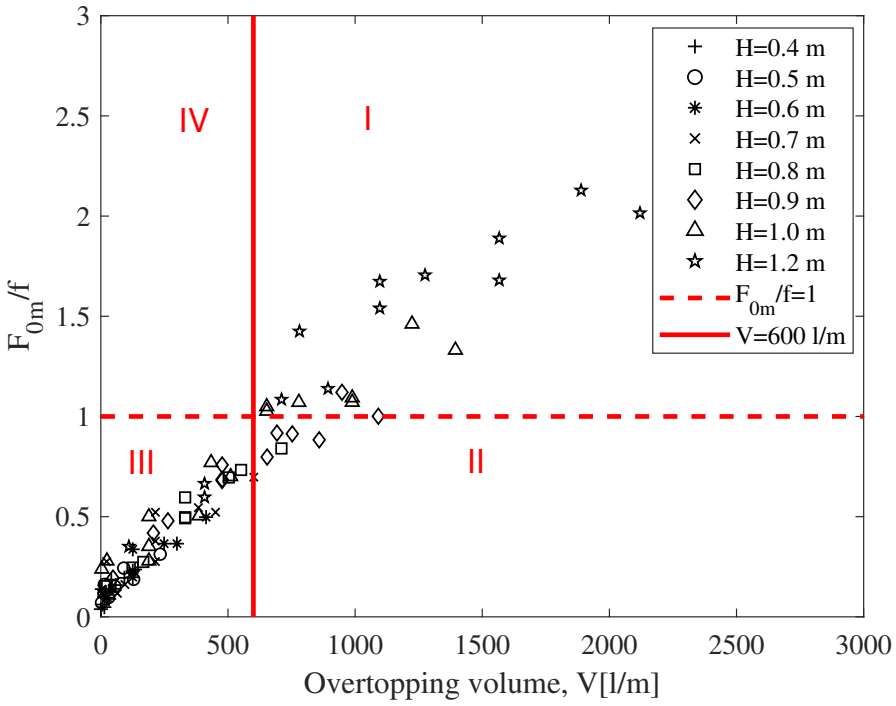
IV
I
III
II
H=0.4 m
H=0.5 m
H=0.6 m
H=0.7 m
H=0.8 m
H=0.9 m
H=1.0 m
H=1.2 m
F0m/f=1
V=600 l/m
F0m/f
Overtopping volume, V[l/m]
0
0.5
1
1.5
2
2.5
3
0
500
1000
1500
2000
2500
3000

Appendix A. Prediction of overtopping volume

The volume of overtopping flow (V, m^3/m) is defined as the volume of overtopping water per unit flow's width over one wave cycle (averaged over several cycles in the time window of valid measurements as defined in Section 3.4), which is measured using CG5 located inside the overtopping tank (volume of overtopping flow equals the elevation measurement by CG5 multiplied by length of the collection tank).

EurOtop (2018) summarized some formula to estimate the maximum overtopping volume for irregular incident waves within a storm duration. While there is no existing formula for predicting V for a regular wave, the experiment data consisting of 70 data points in the present study show that V almost linearly increases with d_{0m}^2, as shown in Fig. A1. The best fit to the data gives:

$$V = 7.756{d_{0m}}^2 \tag{A.1}$$

Note that Eq. (A.1) is only applicable to 1:3 slope. To apply Eq. (A.1), a predictor of d_{0m} is required, which has been derived in Section 4.2.2.

Figure A1:

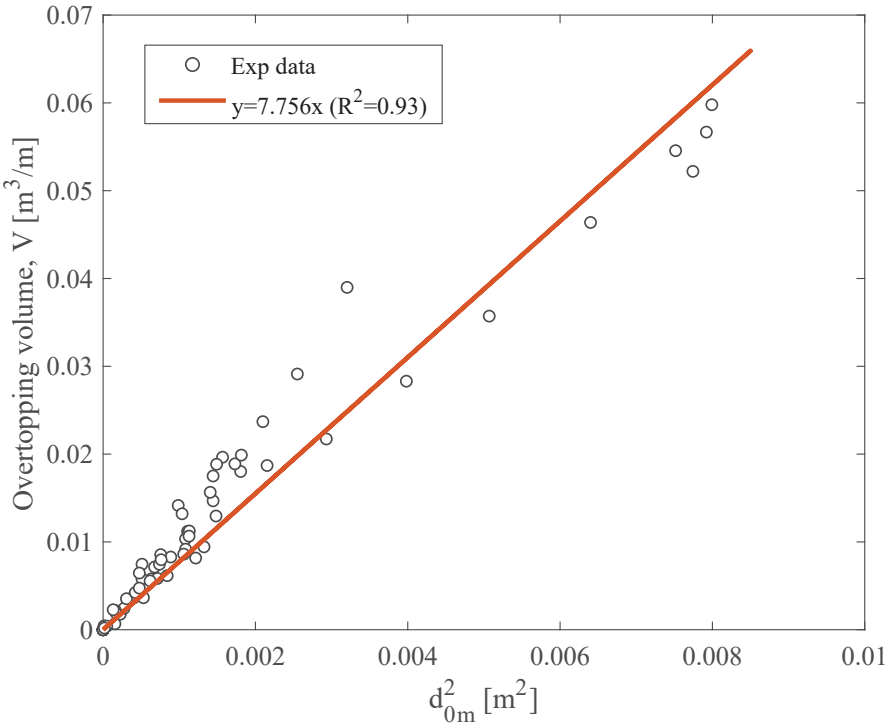
Exp data
y=7.756x (R2=0.93)
Overtopping volume, V [m3/m]
d2 0m [m2]
0.07
0.06
0.05
0.04
0.03
0.02
0.01
0
0.002
0.004
0.006
0.008
0.01